NTIA Report 99-368

# Medium Frequency Propagation Prediction Techniques and Antenna Modeling for Intelligent Transportation Systems (ITS) Broadcast Applications

**Nicholas DeMinco**

**U.S. DEPARTMENT OF COMMERCE**
**William M. Daley, Secretary**

Larry Irving, Assistant Secretary
for Communications and Information

August 1999

AUTHENTICATED U.S. GOVERNMENT INFORMATION GPO

This Page Intentionally Left Blank

This Page Intentionally Left Blank

CONTENTS

Page

FIGURES . . . . . v

ABSTRACT . . . . . 1

1. INTRODUCTION . . . . . 1

2. BASIC CONCEPTS IN RADIO-WAVE PROPAGATION . . . . . 3

3. GROUND-WAVE PROPAGATION . . . . . 4

3.1 SPECIFIC GROUND-WAVE PROPAGATION MODELS . . . . . 8

4. SKY-WAVE PROPAGATION . . . . . 20

5. ANTENNA MODELING . . . . . 29

6. SYSTEM PERFORMANCE CALCULATIONS AND PREDICTIONS . . . . . 42

7. CONCLUSION . . . . . 57

8. REFERENCES . . . . . 61

This Page Intentionally Left Blank

This Page Intentionally Left Blank

FIGURES

Page

Figure 1. Spherical smooth-Earth geometry. . . . . 10

Figure 2. Spherical smooth-Earth mixed-path geometry. . . . . 15

Figure 3. Geometry for integral equation irregular-Earth model along the great circle path. . . 19

Figure 4. Elevation plane pattern for a quarter-wave monopole on a ground screen. . . . . 22

Figure 5. FCC/Region 2 sky-wave curve of median field strength versus distance . . . . . 24

Figure 6. ITU sky-wave curves of median field strength for several values of geomagnetic latitiude at 1000 kHz. . . . . 27

Figure 7. Wang sky-wave curves of median field strength for several values of geomagnetic latitude. . . . . 28

Figure 8. Space wave and unattenuated surface wave components of the ground wave for a vertical dipole at the Earth's surface for average ground conditions at 760 kHz. . . . 31

Figure 9. Elevation plane pattern for the space wave antenna power gain for the DGPS transmitter site antenna for average ground conditions at 300 kHz. . . . . 34

Figure 10. Electric field strength antenna patterns of the space wave and the surface wave for the DGPS transmitter site for average ground conditions at 300 kHz. . . . . 35

Figure 11. Power gain antenna pattern in the elevation plane for the space wave for the DGPS one meter whip mounted in the center of the van roof for average ground conditions at 300 kHz. . . . . 36

Figure 12. Power gain antenna pattern in the elevation plane for the space wave for the one meter whip antenna mounted in the center of the van roof for average ground conditions at 760 kHz. . . . . 37

Figure 13. Power gain antenna pattern in the elevation plane for a quarter-wave monopole antenna on a ground screen for average ground conditions at 760 kHz. . . . . 38

Figure 14. Equivalent gain antenna pattern for station KTLK nighttime antenna configuration versus azimuth angle for average ground conditions at 760 kHz. . . . . 39

Figure 15. Equivalent gain antenna pattern for station KTLK daytime antenna versus azimuth angle for average ground conditions at 760 kHz. . . . . 40

Figure 16. Power gain antenna pattern in the elevation plane on azimuth beam maximum For the KTLK nighttime antenna for average ground conditions at 760 kHz. . . . . 41

Figure 17. Power gain antenna pattern in the elevation plane on azimuth beam maximum for the KTLK daytime antenna for average ground conditions at 760 kHz. . . . . 41

Figure 18. Predicted KTLK day coverage contours (dBuV/m) using the smooth-Earth model. . . . . 44

Figure 19. Predicted KTLK day coverage contours (dBuV/m) using the smooth-Earth mixed-path model. . . . . 45

Figure 20. Predicted KTLK night coverage contours (dBuV/m) using the smooth-Earth model. . . . . 46

Figure 21. Predicted KTLK night coverage contours (dBuV/m) using the smooth-Earth mixed-path model. . . . . 47

Figure 22. Electric field strength vs distance from station KTLK at nighttime on 330 degree radial using the smooth-Earth model. . . . . 49

Figure 23. Electric field strength vs distance from station KTLK at nightttime on 330 degree radial using the smooth-Earth mixed-path model. . . . . 50

Figure 24. Comparison of measured and predicted DGPS field strength for the Appleton to Pendleton path. . . . . 51

Figure 25. Terrain contour for path from Appleton to Pendleton, Washington. . . . . 52

Figure 26. Comparison of measured and predicted data for Canyonlands, Utah path at 520 kHz. . . . . 53

Figure 27. Comparison of measured and predicted data for Canyonlands, Utah path at 1618 kHz. . . . . 54

Figure 28. Terrain contour for Canyonlands, Utah measurement site. . . . . 55

Figure 29. Contours of electric-field strength in dBuV/m from the Appleton, WA DGPS site at nighttime (f=300 kHz). . . . . 56

Figure 30. Contours of electric-field strength in dBuV/m from the Appleton, WA DGPS site at daytime (f=300 kHz). . . . . 57

This Page Intentionally Left Blank

This Page Intentionally Left Blank

# MEDIUM FREQUENCY PROPAGATION PREDICTION TECHNIQUES AND ANTENNA MODELING FOR INTELLIGENT TRANSPORTATION SYSTEMS (ITS) BROADCAST APPLICATIONS

Nicholas DeMinco*

This paper discusses the basic aspects of radio-wave propagation and antenna modeling in the medium frequency (MF) band. This band covers the frequencies of 300 to 3000 kHz. More specifically, we are concerned with the ground wave and the sky wave in the 300 kHz to 1705 kHz band. The sky wave models described in this paper are valid from 150 kHz to 1705 kHz. The ground wave models described in this paper are valid from 10 kHz to 30 MHz. The AM Broadcast band of 535 to 1605 kHz is in this band and is planned to be used in the Advanced Traveler Information Systems (ATIS) of Intelligent Transportation Systems (ITS) for rural travelers. This system would provide information such as road conditions, road hazards, weather, and incident reporting. The 285 kHz to 325 kHz band is presently being used for a differential correction signal in another application of ITS called the Differential Global Positioning System (DGPS) that will be used for precision location of vehicles. The propagation of radio waves in this band depends on both a ground wave and a sky wave and is quite different from propagation at any other frequency. Antenna modeling in this band is also quite unlike that in other bands. This paper describes radio wave propagation together with antenna modeling in this frequency band so that a better understanding of the phenomena can be obtained for use in design and application of ITS subsystems. The models described here can be used for designing systems and making performance predictions for both of these ITS applications and any other systems that operate in this band. The paper contains descriptions of both sky-wave and ground-wave propagation models in addition to the methodology used to analyze antennas that operate in this band. A method of calculating and normalizing antenna gain for MF systems computations is also discussed. Some comparisons of measured and predicted data are also contained in the descriptions.

Keywords: radio-wave propagation, antennas, communications, intelligent transportation systems

## 1. INTRODUCTION

This paper contains discussions about radio-wave propagation and antenna analysis in the medium frequency (MF) band and how analysis methods differ from those used in other frequency bands. The MF band covers the frequencies of 300 to 3000 kHz. Actually the sky-wave propagation models are also valid down to 150 kHz, and the ground-wave model is valid down to 10 kHz. The paper specifically addresses two applications of Intelligent Transportation Systems, but this material is

*The author is with the Institute for Telecommunication Sciences, National Telecommunication and Information Administration, U.S. Department of Commerce, Boulder, CO 80303.

useful for other systems that operate in this band. Radio-wave propagation prediction models, that can be used for engineering analyses of communication systems, determine the basic transmission loss between a communications transmitter and receiver. This knowledge is necessary for the prediction of the behavior of separate functional communication subsystems of the Intelligent Transportation System (ITS) and other systems operating in this band. This knowledge can be used for planning, architectural evaluation, system performance prediction, system design and testing, interference resolution, and standards development. The AM Broadcast band of 535 to 1605 kHz is in this band and is planned to be used in the Advanced Traveler Information Systems (ATIS) of ITS for rural travelers. This system would provide information like road conditions, road hazards, weather, and incident reporting. The subsystems of ITS use computer and telecommunications technology to provide information to travelers about road and transit travel conditions and also provide information to monitor, guide, and control the operation of vehicles. ITS can improve safety, reduce congestion, enhance mobility, minimize environmental impact, save energy, and promote economic productivity on the Nation's transportation system. The 285 kHz to 325 kHz band is presently being used for a differential correction signal in another application of ITS called the Differential Global Positioning System (DGPS) that will be used for precision location of vehicles. The DGPS signals in this band are used to differentially correct the location determined by the Global Positioning System (GPS) navigation system. Each DGPS site processes information from the GPS satellite signal to calculate the location. The DGPS site then compares this location to its exact fixed location and sends out a correction signal at 300 kHz for others to obtain a more precise location calculation than originally available from the L-band GPS satellite signals.

Propagation models that are used to analyze radio communication systems require sound engineering judgement in their use for a particular analysis. For the MF band of 300 kHz to 3000 kHz both the ground wave and the sky wave must be considered. The propagation of radio waves in this band depends on both a ground wave and a sky wave and is quite different from propagation at any other frequency. Antenna modeling in this band is also quite unlike that in other bands. The expected sky-wave signal combined with the ground-wave signal may be compared with the expected radio noise environment (consisting of atmospheric, galactic, and man-made noise components) to predict the likelihood that the communication link will operate satisfactorily. The presence of the sky wave at night could create potential interference problems between distant stations on the same frequency or frequencies that are near each other. The sky-wave models provide some means of estimating the expected field strengths of signals to assist in frequency allocation and to avoid potential interference problems. Free space loss cannot be used to characterize radio-wave propagation at these frequencies. Other propagation models must be used to predict radio-wave propagation correctly. The ground-wave prediction methods presented here are valid from 10 kHz to 30 MHz.

The sky-wave propagation loss prediction methods discussed in this paper are valid from 150 kHz to 1705 kHz. Above 1705 kHz and below 150 kHz there are different sky-wave propagation phenomena that take place and other methods must be used which are not included in this paper, since our current attention focuses on frequencies around 300 kHz and the AM broadcast band.

This paper will describe analysis techniques and propagation models used in this frequency band and will give examples of comparisons of predictions and measurements. Use of the appropriate antenna

gains with the propagation models is also essential to accurate performance prediction. This paper will also explain how antenna gains are determined at these MF frequencies to predict system performance correctly. A method of calculating and normalizing antenna gain for systems computations has been proposed. Antenna modeling examples will be presented for the average frequency of 300 kHz used for DGPS, and the 760 kHz test frequency used for the AM subcarrier Advanced Traveler Information Systems (ATIS) test program.

## 2. BASIC CONCEPTS IN RADIO-WAVE PROPAGATION

In all of the radio-wave propagation concepts that are discussed, it is assumed that the propagation is taking place in the far field of the transmitter and receiver antennas. If a point source radiates power with a transmitter antenna that has a directional gain, then the received power for a receiver antenna is given by the following [1-4]:

$$P_r = P_t + G_t + G_r - L_{fsb} \qquad (dBm) \tag{1}$$

where $P_r$ and $P_t$ are the received and transmitted powers respectively in dBm, and $G_r$ and $G_t$ are the receiver and transmitter antenna gains respectively in dB. $L_{fsb}$ is the free-space basic transmission loss in dB and is given by the following [5]:

$$L_{fsb} = 32.45 + 20 \log(f_{GHz}) + 20 \log(r) \qquad (dB) \tag{2}$$

where $f_{GHz}$ is the frequency of the radio wave in GHz and $r$ is the distance between the transmitter and receiver in meters. Free-space loss is a theoretical reference or limit, against which the actual basic transmission loss $L_b$ can be compared or expressed as a ratio.

Equation (1) can be used to calculate the received power for a transmitter and receiver located in free space. Free space is a highly idealized environment and is not the situation for ITS propagation channels. In the ITS environment there is at least a conducting ground to consider and in many situations the wave may have to propagate through a very complicated environment. For example, the energy may have to propagate: through or be reflected from precipitation, through an atmosphere with oxygen and water vapor, through buildings, around corners, down side streets, into and around wooded areas, and over rough terrain. For radio-wave propagation at MF the loss due to precipitation or atmospheric absorption by water vapor or oxygen is negligible, but the signal must still diffract around obstacles in the environment. Radio-wave propagation at frequencies between 150 kHz and 1705 kHz depends on both a ground wave and a sky wave. Neither of these two wave-propagation phenomena behave like free-space loss. In this type of environment the received signal can be expressed by the simple equation given in (1) if the free-space basic transmission loss $L_{fsb}$

were replaced by the basic transmission loss $L_b$ computed by propagation models that take all of these propagation effects into account. Basic transmission loss is the transmission loss that would occur if the transmitter and receiver antennas were replaced by ideal isotropic loss-free antennas with the same polarization as the real antennas [3,4].

This paper describes the different types of radio-wave propagation phenomena and antenna behavior that must be considered for general radio-wave propagation models in the roadway environment in the MF band. Radio-wave propagation prediction models generally compute basic transmission loss $L_b$ which is combined with antenna gains and transmitter power to perform engineering analyses of communication systems.

## 3. GROUND-WAVE PROPAGATION

The ground-wave signal can be determined using one of several models [6,7] that specifically address the propagation phenomena at these frequencies. One general ground-wave model [6] computes propagation loss, electric field strength, received power, noise, received signal-to-noise power ratio, and antenna factors over lossy Earth. The smooth-Earth and irregular-Earth (terrain dependent) propagation loss prediction methods within this model can be used over either homogeneous or mixed paths. This model combines three propagation loss prediction methods for both smooth and irregular Earth, and an antenna algorithm into a single analysis tool. The propagation loss prediction methods for the ground-wave model compute basic transmission loss and are valid from 10 kHz to 30 MHz. A model that incorporates the sky wave with the ground wave [7] specifically addresses the 150 kHz to 1705 kHz frequency range. The frequency limits of this model have been set by the valid frequency range of the sky-wave model. This model was previously available on a mainframe computer but now operates in a Windows environment on a PC.

The ground wave includes the direct line-of-sight space wave, the ground-reflected wave, and the Norton surface wave that diffracts around the curved Earth. The Norton surface wave will hereafter be referred to as a surface wave in this paper. Propagation of the ground wave depends on the relative geometry of the transmitter and receiver location and antenna heights. The radio wave propagates primarily as a surface wave when both the transmitter and receiver are near the Earth in wavelengths, because the direct and ground-reflected waves in the space wave cancel each other and as a result the surface wave is the only wave that is left. This cancellation is a result of the fact that the elevation angle is zero and the two waves (direct and reflected) are equal amplitude and opposite in phase. This is the condition that exists for the MF band. The surface wave is predominantly vertically polarized, since the ground conductivity effectively shorts out most of the horizontal electric field component. What is left of the horizontal component is attenuated at a rate many times that for the vertical component of the field. When one or both antennas are elevated above the ground to a significant height with respect to a wavelength, the space wave predominates.

The ground-wave propagation phenomena at these frequencies are basically deterministic processes. The noise, however, is a stochastic process. The surface wave propagates along and is guided by the Earth's surface. This is similar to the way that an electromagnetic wave is guided along a

transmission line. Charges are induced in the Earth by the surface wave. These charges travel with the surface wave and create a current in the Earth. The Earth carrying this current can be represented by a leaky capacitor (a resistance shunted by a capacitive reactance). The characteristics of the Earth as a conductor can therefore be represented by this equivalent parallel RC circuit, where the Earth's conductivity can be simulated with a resistor and the Earth's dielectric constant by a capacitor. As the surface wave passes over the surface of the Earth, it is attenuated as a result of the energy absorbed by the Earth due to the power loss resulting from the current flowing through the Earth's resistance. Energy is taken from the surface wave to supply the losses in the ground, and the attenuation of this wave is directly affected by the ground constants of the Earth along which it travels [8].

The attenuation function is the ratio of the electric field from a short dipole over the lossy Earth's surface to that field from the same short dipole located on a flat perfectly conducting surface. At distances within the line of sight the surface wave field strength, *E,* is given by [8]:

$$E = \frac{AE_0}{d} \tag{3}$$

where $E_o$ is the electric field strength of the surface wave at the surface of the Earth at a small distance on the order of a few wavelengths away from the transmitting antenna (the Earth's losses are negligible at this small distance, so this could also be considered the field from the short dipole located on a flat perfectly conducting surface), *d* is the distance between the transmitting antenna and reception point, and *A* is the flat-Earth attenuation function that takes into account the ground losses.

The exact equation derived by Norton [10] for the flat-Earth attenuation function is described later in this paper. Norton further simplified this exact equation into a form that is more amenable to calculation. These simplified expressions for the Norton approximations to the flat-Earth attenuation [9,10] function can be easily implemented on a programmable calculator. They are reasonably accurate for line-of-sight propagation [11].

For $p_o \leq 4.5$ and all *b*:

$$A = e^{-.43p_o + .01p_o^2} - (\sqrt{p_o/2})(\sin b)(e^{-5/8p_o}) \tag{4}$$

For $p_o > 4.5$ and all *b*:

$$A = \frac{1}{2p_o - 3.7} - (\sqrt{p_o/2})(\sin b)(e^{-5/8p_o}) \tag{5}$$

where for vertical polarization:

$$p_o = \frac{\pi R(km)\,[f(MHz)]^2 \cos b}{(54x10^2)\sigma}$$
$$b = \tan^{-1}\frac{(\varepsilon_r + 1) f(MHz)}{18x10^3 \sigma} \qquad (6)$$

and for horizontal polarization:

$$p_o = \frac{\pi R(km) 6x10^4 \sigma}{\cos b'}$$
$$b' = \tan^{-1}\frac{(\varepsilon_r - 1) f(MHz)}{18x10^3 \sigma} \qquad (7)$$

where $\sigma$ is the conductivity of the Earth in siemens per meter, and $\varepsilon_r$ is the relative permittivity of the Earth. The field strength at this small distance is directly proportional to the square root of power radiated by the transmitter and the directivity of the antenna in the horizontal and vertical planes. If the antenna is non-directional in the horizontal plane and has a vertical directional pattern that is proportional to the cosine of the elevation angle (this corresponds to a short vertical antenna), then the electric field at one kilometer for an effective radiated power of one kilowatt is 300 mV/m [8]. The flat-Earth attenuation function A is dependent upon frequency, distance, and the ground constants of the Earth along which the wave is traveling. A numerical distance, $p_o$ (equations (6) and (7) above) can be computed that is a function of frequency, ground constants, and distance in wavelengths. If the numerical distance is less than one, then the attenuation function is very close to one, and as a result for distances close to the transmitting antenna, the losses in the Earth have very little effect on the electric-field strength of the surface wave. In this region, the electric field strength is inversely proportional to distance. For situations where the numerical distance becomes greater than unity, the attenuation function decreases in magnitude rapidly. When the numerical distance becomes greater than 10, the attenuation factor is also inversely proportional to distance. The combination of the attenuation factor and the unattenuated electric field both being inversely proportional to distance results in the electric field strength of the surface wave being inversely proportional to the square of the distance when the numerical distance is greater than 10.

At lower HF frequencies, AM broadcast (medium frequencies), and lower frequencies in the LF band (below 300 kHz), the Earth can be regarded as being purely resistive in nature. The equivalent circuit of the Earth is still a resistor of resistance R and capacitor of capacitance C in parallel. However, the Earth is predominantly resistive at these frequencies because of the fact that more current flows through the resistance, because $R << 1/\omega C$, so under these conditions the resistor has the major effect. The attenuation factor is then primarily dependent on the conductivity of the Earth and the frequency. For frequencies above about 10 MHz, the impedance represented by the ground

is primarily capacitive, so the attenuation factor for the surface wave at a given physical distance is determined by the dielectric constant of the Earth and the frequency.

The attenuation of the surface wave is determined by the average values of the Earth conductivity and dielectric constant down to a depth to which the ground currents penetrate and still maintain an appreciable magnitude. This is similar to a skin depth phenomenon in a good conductor. The depth of penetration of the surface wave currents depends upon frequency, dielectric constant, and conductivity. This ranges from a fraction of a meter at the highest frequencies for HF communications to tens of meters at AM broadcast and lower frequencies. For this reason propagation at the lower frequencies is not particularly dependent on conditions at the actual surface of the ground. Therefore, a recent rainfall would not significantly affect propagation at MF and LF frequencies.

The depth of penetration of an electromagnetic wave into the surface of the Earth depends upon the frequency and ground constants of the Earth. The electric field strength at a distance z below the surface of the Earth is given by [12]:

$$E = E_o e^{-\alpha z} \tag{8}$$

where $E_o$ is the electric field intensity at the surface of the Earth, $z$ is the depth below the surface of the Earth, and $\alpha$ is the attenuation per meter of the electric field intensity.

The attenuation per meter $\alpha$ is given by:

$$\alpha = \omega\sqrt{\mu\varepsilon}\sqrt{1/2\sqrt{1+(\sigma/\omega\varepsilon)^2}-1/2} \tag{9}$$

where $\omega$ is the angular frequency and is equal to $2\pi f$, $f$ is radio frequency in Hertz, $\mu$ is the magnetic permeability of the Earth $\mu = \mu_r \times 4\pi \times 10^{-7}$ henries/meter, $\mu_r$ is the relative permeability, $\varepsilon$ = the permittivity of the Earth = $\varepsilon_r \bullet (8.85 \times 10^{-12})$ farads per meter, $\varepsilon_r$ is the relative permittivity of the Earth, and $\sigma$ is the conductivity of the Earth in siemens per meter.

The distance the wave must travel in a lossy medium to reduce its amplitude to $e^{-1}$ =.368 of its value at the surface is $\delta = 1/\alpha$ meters and is called the skin depth of the lossy medium. For other values of attenuation of the electric field, $r=e^{-\alpha z}$, one can use $\alpha$ to determine the distance $z$ below the surface where the electric field is attenuated to that ratio $r$. The ratio $r$ is always less than or equal to 1. The distance $z$ is given by:

$$z = -\frac{\ln r}{\alpha} \tag{10}$$

where ln$r$ is the natural logarithm of $r$. An example is where $f$=300 kHz, $\mu_r$= 1 for a nonmagnetic Earth, $\varepsilon_r$= 15 for average ground, $\sigma$ = .005 for average ground. The attenuation $\alpha$ is calculated as .0751 per meter and $\delta$ is calculated as $1/\alpha$ as 13.32 meters.

This is the distance at which the electric field is $e^{-1}$ or .368 (36.8 percent) of its value at the surface of the Earth. If the distance $z$ at which the electric field is .1 (10 percent) of its value at the surface is desired, then ln $r$ is ln (.1)= -2.3026, and $\alpha$ = .0751, so $z$= $-1/\alpha$ (-2.3026) = 30.66 meters. Table 1 gives the depth of penetration for $f$= 300 kHz.

Table 1. Depth of Penetration in the Earth for Different Ground Conditions

| Conductivity (siemens/m) | Permittivity (no units) | Media Type | Alpha ($\alpha$) (per meter) | Skin Depth ($\delta$) for $r=e^{-1}$=.368 (meters) |
|---|---|---|---|---|
| 0.001 | 4.0 | poor ground | 0.0333 | 30.04 |
| 0.005 | 15.0 | avg. ground | 0.0751 | 13.32 |
| 0.020 | 25.0 | good ground | 0.1523 | 06.57 |
| 0.010 | 81.0 | fresh water | 0.1017 | 09.83 |
| 5.000 | 81.0 | sea water | 2.4330 | 00.41 |

## 3.1 Specific Ground-wave Propagation Models

### 3.1.1 The Smooth-Earth Model

The simplified expressions for field strength of a ground wave described previously in equations (3) through (7) are only valid for line-of-sight radio-wave propagation. The antennas must also be located on the ground or very near it in distance with respect to a wavelength. They are the simplified expressions for the Norton [10] approximation to the Sommerfeld flat-Earth attenuation function. Sommerfeld originally solved the problem of radiation over a flat lossy Earth for a short current element in 1909 [13]. Later work by Sommerfeld and many others resulted in an extensive numerical evaluation of the flat-Earth attenuation function. One of the more prominent evaluations of the flat-Earth attenuation function was that due to Norton [9,10]. When the geometry of the receiver antenna, transmitter antenna, and the Earth are such that a flat-Earth attenuation function [14] is no longer valid, then other methods must be used. In this paper a smooth-Earth model is described that uses a variety of algorithms to account for this geometry. The smooth-Earth model described in this paper is that developed by L.A. Berry [15]. It is also described in more detail in [6,7,14,16,17,18]. The following six computation techniques are used in this smooth-Earth model to account for all possible propagation geometries: flat-Earth attenuation function, flat-Earth attenuation function with a curvature correction, the power series expansion, the residue series calculation, geometric optics, and numerical integration of the full-wave theory. The appropriate technique is selected according to the relative geometry of the transmitter and receiver antenna heights and locations with respect to the Earth. Diffraction is included where necessary in the last five of these techniques.

The details of the smooth-Earth model equations are given in Berry [15] and Stewart, et al. [16]. Some of the basic equations will be summarized in this section. Figure 1 describes the geometry for a spherical smooth Earth. The flat-Earth attenuation function is used for line-of-sight propagation when the path is short and the Earth can be assumed to be flat [19]. If in addition, the transmitter and receiver antennas are near the Earth with respect to a wavelength, then the flat-Earth attenuation function [19] is used and the electric-field strength *E(d)* in V/m is given by [15,16,19,20]:

$$E(d) = \frac{9.487\sqrt{P_E}\ A(\rho)}{d} \tag{11}$$

where $P_E$ is the effective radiated power in watts, $d$ is the distance between the transmitter and receiver in kilometers, and $A(\rho)$ is the flat-Earth attenuation function. The equations (3) through (7) given earlier for the flat-Earth attenuation function $A$ are an approximation to $A(\rho)$. The following equations are the more precise expressions used to predict ground-wave loss [13,19]:

$$A(\rho) = 1 - R_0 \Delta e^{\rho^2} \operatorname{erfc}(\rho) \tag{12}$$

$$\begin{aligned} R_0 &= e^{j\pi/4}\sqrt{\pi kD/2} \\ D &= \sqrt{d^2 + (h_1 - h_2)^2} \end{aligned} \tag{13}$$

$$\rho = e^{j\pi/4}\sqrt{kD/2}\,\Delta\left(1 + \frac{(h_1 + h_2)}{\Delta D}\right) \tag{14}$$

where $d = a\theta$ (Figure 1) is the great circle path distance between the transmitter and the receiver base locations, $h_1$ and $h_2$ are the heights of the transmitter and receiver antennas respectively, $D$ is the line of sight distance between the transmitter and the receiver, and $k = 2\pi/\lambda$, and erfc($\rho$) is the complementary error function [21].

The surface impedance of the ground is given by $\Delta$. If the polarization is vertical, then $\Delta$ is:

$$\Delta = \frac{\sqrt{\varepsilon_{gc} - 1}}{\varepsilon_{gc}} \tag{15}$$

If the polarization is horizontal, then $\Delta$ is:

$$\Delta = \sqrt{\varepsilon_{gc} - 1} \tag{16}$$

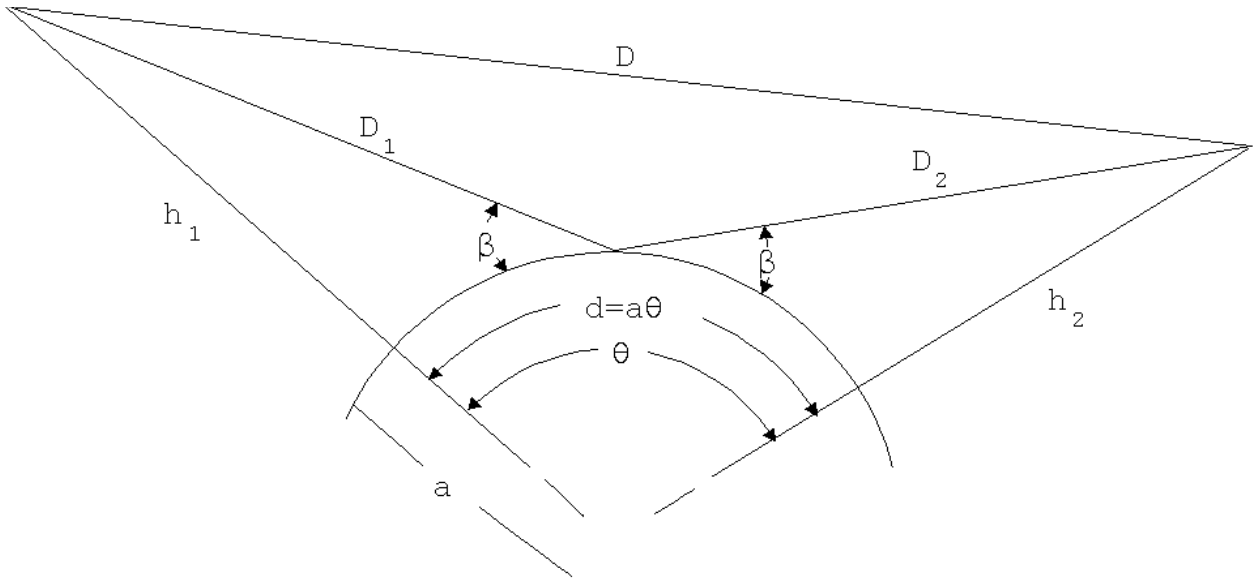



Figure 1. Spherical smooth-Earth geometry.

$$\varepsilon_{gc} = \varepsilon_g + \frac{\sigma_g}{j\omega\varepsilon_o} \tag{17}$$

where $\varepsilon_g$ is the relative dielectric constant of ground, $\sigma_g$ is the conductivity of the ground in siemens per meter, $\varepsilon_o$ is the permittivity of free space, 8.85 x $10^{-12}$ farads per meter, $\omega = 2\pi f$, and $f$ is the operating frequency in Hertz. The surface impedance, $\Delta$, is a function of the ground constants of the Earth's surface.

When the transmitter and receiver antenna locations are high enough such that an observer positioned at either the receiver or transmitter location is well above the radio horizon when viewed from the other, the field strength computation involves the use of geometrical optics [15,16]. The electric field $E$ in V/m is given by:

$$E = 9.487\sqrt{P_E}\frac{e^{-jk(D-d)}}{2D}\left(1 + R_g e^{-jk(D_1+D_2-D)}\right) \tag{18}$$

where $R_g$ is the appropriate ground reflection coefficient for vertical or horizontal polarization. The direct line-of-sight distance $D$ between the transmitter and receiver antennas is given by [15,16]:

$$D=\sqrt{[2a^2+2a(h_1+h_2)](1-\cos\theta)+h_1^2+h_2^2-2h_1h_2\cos\theta} \tag{19}$$

The radius of the Earth is denoted as $a$. Closed form solutions for $D_1$ and $D_2$ are not possible, but Stewart et al. [16] gives details on calculating these distances using an iterative method.

When the receiving antenna is near the radio horizon of the transmitting antenna, but not beyond it, then the field depends on diffraction effects in addition to the direct wave, and in this case the computation is performed by numerical integration of the full-wave theory integral [15]. The expression for calculating the electric field using the full-wave theory integral is [15,16,19]:

$$E=9.487\sqrt{P_E}\sqrt{\frac{v}{12\sin\theta}}\frac{e^{j3\pi/4}}{a}\int_\Gamma e^{-jkt}F_I(q,t)\,dt \tag{20}$$

where $v=(ka/2)^{1/3}$, $x=v\theta$, and $q=-jv\Delta$. $\Gamma$ is a contour enclosing the poles of $F_1(q,t)$.

$$F_I(q,t)=\frac{H_1(h_1)H_2(h_2)}{\frac{W_1'(t)}{W_1(t)}-q} \tag{21}$$

$H_1(h_1)$ and $H_2(h_2)$ are height gain functions given by:

$$H_1(h)=\frac{W_1(t-y)}{W_1(t)} \tag{22}$$

$$H_2(h_2)=-0.5jW_2(t-y)\,[W_1'(t)-qW_1(t)]-W_1(t-y)\,[W_2'(t)-qW_2(t)] \tag{23}$$

where $y=kh_i/v$, and $W_1'(t)$ denotes the differential of $W_1(t)$ with respect to $t$. The functions $W_n(t)$ are Airy functions [19] that satisfy the differential equation:

$$\begin{aligned} W_n''(t)&=tW_n(t)\\ W_1(t)&=\frac{1}{\sqrt{\pi}}\int_{\Gamma_1}e^{(st-s^3/3)}ds\\ W_2(t)&=\frac{1}{\sqrt{\pi}}\int_{\Gamma_2}e^{(st-s^3/3)}ds \end{aligned} \tag{24}$$

where the contour $\Gamma_1$ is taken as the straight line segment from $\infty e^{j2\pi/3}$ to the origin and out along the

real axis to $\infty$, and contour $\Gamma_2$ is taken as the straight line segment from $\infty e^{-j2\pi/3}$ to the origin and out along the real axis to $\infty$.

The poles of the function $F_1(q,t)$ occur at points $t_i$ and they satisfy the differential equation [19,22]:

$$W_1'(t) - qW_1(t) = 0 \tag{25}$$

For long paths, the Earth cannot be considered flat. If, in addition, the geometry is such that a straight line connecting the transmitter and receiver antennas intersects the curved Earth so that the transmitter and receiver antennas are beyond line of sight of each other and propagation is beyond the horizon, then the full-wave theory integral must be evaluated using the residue series [19,22]. It is necessary to calculate the series by summing the residues at the poles $t_i$ of $F_1(q,t)$ in equation (21) above [19,22]. The electric field is given by [19]:

$$E = 9.487\sqrt{P_E}\frac{\pi}{a}\sqrt{\frac{2v}{6\sin\theta}}e^{-j\pi/4}\sum_i e^{-jxt_i}\frac{H_1(h_1)H_1(h_2)}{t_i - q^2} \tag{26}$$

For cases where the antennas are close to the Earth and the path lengths are long enough such that the Earth cannot be considered flat, the field-strength computation is performed using either a flat-Earth attenuation function with a small-Earth curvature correction or a power series expansion. These two techniques reduce the need to use the numerical integration of the full-wave theory integral (equation 20), since it is a very time consuming computation [23]. These two techniques bridge the gap for loss computation between the case where the Earth is flat (flat-Earth attenuation function) and that where the receiving antenna is near the radio horizon of the transmitting antenna.

The computation technique (either flat-Earth attenuation function with curvature correction or power series expansion) is selected depending on whether the magnitude of the factor $q$ (already defined) is small or large [24]. Recall that $q$ is given by:

$$q = -j(ka/2)^{1/3}\Delta \tag{27}$$

where $k=2\pi/\lambda$, $\lambda$ is the wavelength of the radio wave in meters, $a$ is the radius of the Earth in meters, and $\Delta$ is the normalized surface impedance of the ground below the antenna in question. The expressions for $\Delta$ are the same as given in equations (15) through (17). The surface impedance $\Delta$ is a function of the ground constants of the Earth's surface.

If the magnitude of $q$ is small (<0.1), then a power series expansion is used for the attenuation function $f(x)$. The electric field $E$ at a great circle distance $d$ on the Earth's surface is $E_0 \bullet f(x)$. $E_0$ is the electric field of the same dipole source located on a flat perfect conductor. The power series expansion for $f(x)$ for small q (<0.1) is given by [24-30]:

$$f(x) = \sum_{m=0}^{\infty} A_m[e^{j\pi/4}q\,x^{1/2}]^m \tag{28}$$

where

$$x = d/a(ka/2)^{1/3} \tag{29}$$

$$\begin{aligned}
A_0 &= 1 \\
A_1 &= -j\pi^{1/2} \\
A_2 &= -2 \\
A_3 &= j\pi^{1/2}(1 + 1/4q^3) \\
A_4 &= 4/3(1 + 1/2q^3) \\
A_5 &= -j\pi^{1/2}/4(1 + 3/4q^3) \\
A_6 &= -8/15(1 + 1/q^3 + 7/32q^6) \\
A_7 &= j\pi^{1/2}/6(1 + 5/4q^3 + 27/32q^6) \\
A_8 &= 16/105(1 + 3/2q^3 + 27/32q^6 \\
A_9 &= -j\pi^{1/2}/24(1 + 7/4q^3 + 5/4q^6 + 21/64q^9) \\
A_{10} &= -(32/945 + 64/945q^3 + 11/189q^6 + 1/270q^9)
\end{aligned} \tag{30}$$

Higher order coefficients are not available in the literature, but the accuracy is adequate with the coefficients given above [24].

If the magnitude of $q$ is large ($\geq$0.1), then a small curvature expansion is more appropriate for the attenuation function [25,27,28]. The expression for the small curvature expansion is given by:

$$\begin{aligned}
f(x) = F(p) + \frac{1}{4q^3}[1 - j[\pi p]^{1/2} - (1 + 2p)F(p)] + \frac{1}{4q^6}[1 - j[\pi p]^{1/2}(1 - p) - 2p \\
+ \frac{5p^2}{6} + (\frac{p^2}{2} - 1)F(p)]
\end{aligned} \tag{31}$$

$$\begin{aligned}
F(p) &= 1 - j[\pi p]^{1/2} e^{-p} \operatorname{erfc}(jp)^{1/2} \\
p &= jxq^2 \equiv -jkd\Delta^2/2
\end{aligned} \tag{32}$$

The erfc is the complementary error function defined previously [21]. The implementation of these two techniques reduces the need for the numerical integration technique and reduces computation time considerably.

If the terrain contour is “smooth” or the terrain irregularities are much smaller than a wavelength,

then the smooth-Earth method is mathematically and numerically accurate for ground-wave predictions in a frequency range from 10 kHz to 100 MHz; however above 30 MHz the irregularities of the atmosphere make statistical methods more appropriate. All of the models discussed so far are part of the smooth-Earth method.

When the terrain contour is smooth, the smooth-Earth model is valid for all combinations of antenna heights, frequency, and dielectric constants by virtue of the computation techniques contained within its structure. It should be used only out to the maximum distances considered useful for ground-wave propagation at each frequency, since the sky wave will become significant from those distances to points beyond.

### 3.1.2 The Smooth-Earth Mixed-Path Model

A mixed path is one where the ground constants change along the propagation path between the transmitter and receiver. The path can be described by a series of finite length segments, each with different ground constants. The smooth-Earth mixed-path model is a specific sequence of smooth-Earth model runs over each of the segments that are then combined in a particular order as determined by the Millington algorithm [31]. The Millington algorithm is based on reciprocity considerations. This smooth-Earth, mixed-path model is valid for the same frequency and distance ranges as the smooth-Earth method. The antenna heights are set to zero for each smooth-Earth run over each of the segments and combination of segments required by the algorithm. A height-gain function is then applied to the transmitter and receiver antennas using the ground constants under each antenna and the antenna heights. The result is the propagation loss over a mixed path with compensation for antenna heights. The Millington algorithm implemented in the smooth-earth, mixed-path model will be discussed for the three section mixed path of Figure 2. Expansion to more sections is a straightforward process.

The first step involves the calculation of losses using the smooth-Earth model over single sections and combinations of sections using the different ground constants. With a transmitter at T as a source, (Figure 2), compute the loss $L_{tr}$ in decibels (dB).

$$L_{tr}(dB) = L_1(d_1) - L_2(d_1) + L_2(d_1+d_2) - L_3(d_1+d_2) + L_3(d_1+d_2+d_3) \tag{33}$$

where $L_1(d_1)$ is the loss in dB over distance $d_1$ using $\sigma_1$ and $\varepsilon_1$, $L_2(d_1)$ is the loss in dB over distance $d_1$ using $\sigma_2$ and $\varepsilon_2$, $L_2(d_1+d_2)$ is the loss in dB over distance $d_1+d_2$ using $\sigma_2$ and $\varepsilon_2$, $L_3(d_1+d_2)$ is the loss in dB over distance $d_1+d_2$ using $\sigma_3$ and $\varepsilon_3$, and $L_3(d_1+d_2+d_3)$ is the loss in dB over distance $d_1+d_2+d_3$ using $\sigma_3$ and $\varepsilon_3$.

With a transmitter at *R* as a source (Figure 2), compute the loss $L_{rt}$ in decibels.

$$L_{rt}(dB) = L_3(d_3) - L_2(d_3) + L_2(d_3+d_2) - L_1(d_3+d_2) + L_1(d_3+d_2+d_1) \tag{34}$$

where $L_3(d_3)$ is the loss in dB over distance $d_3$ using $\sigma_3$ and $\varepsilon_3$, $L_2(d_3)$ is the loss in dB over

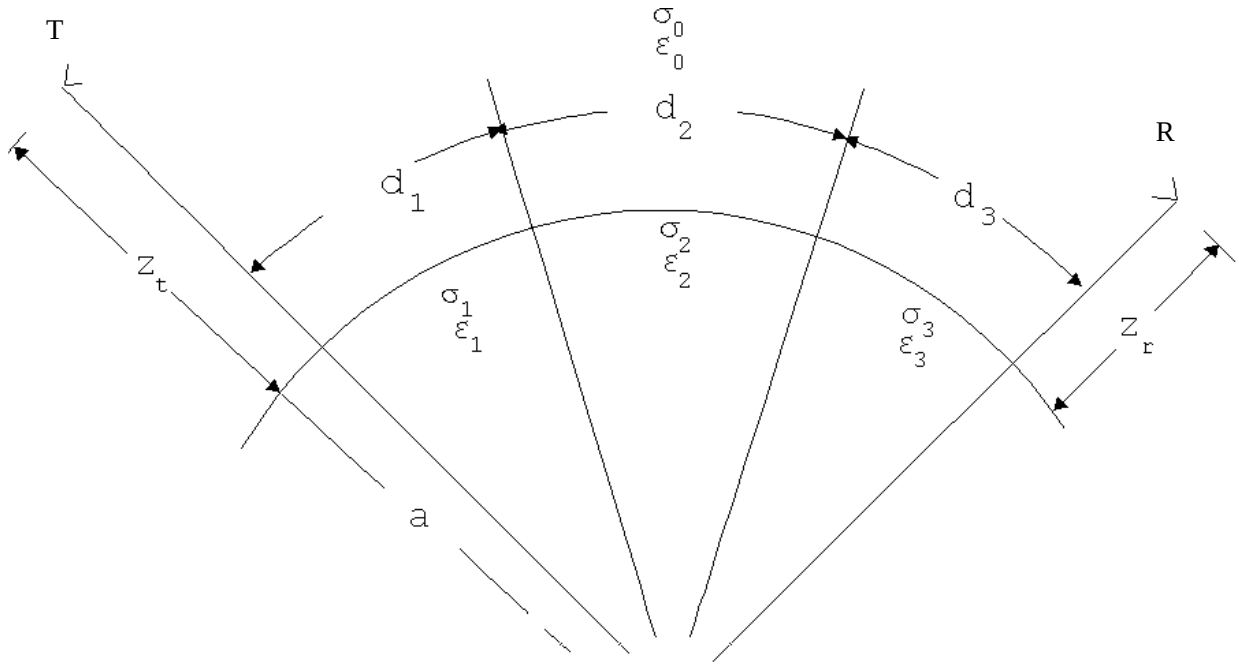



Figure 2. Spherical smooth-Earth mixed-path geometry.

distance $d_3$ using $\sigma_2$ and $\varepsilon_2$, $L_2(d_3+d_2)$ is the loss in dB over distance $d_3+d_2$ using $\sigma_2$ and $\varepsilon_2$, $L_1(d_3+d_2)$ is the loss in dB over distance $d_3+d_2$ using $\sigma_1$ and $\varepsilon_1$, and $L_1(d_3+d_2+d_1)$ is the loss in dB over distance $d_3+d_2+d_1$ using $\sigma_1$ *and* $\varepsilon_1$.

The total loss $L_t(dB)$ is then computed:

$$L_t(dB) = \frac{L_{tr}(dB) + L_{rt}(dB)}{2} - 20\log(|G(z_t)| * |G(z_r)|) \qquad (35)$$

$|G(z_t)|$ and $|G(z_r)|$ denote the magnitude of the height-gain functions for the transmitter and receiver antennas respectively.

The height-gain function is given approximately by the first two terms of the Taylor series expansion for the exact height-gain function arising from the smooth-Earth diffraction series [19,22,28,32]:

$$G(z) = 1 + jk\Delta z \tag{36}$$

where $z$ is the transmitter height, $z_t$, or receiver antenna height, $z_r$, in meters. The factor $k = 2\pi/\lambda$, and $\lambda$ is the wavelength in meters of the radio wave. The normalized surface impedance of the ground below the antenna in question is $\Delta$ as defined previously. The imaginary part of a complex number is denoted by $j$.

The function is valid up to about the first maximum in the height-gain pattern [19,29]. This height gain function is used in the smooth-Earth mixed-path model and the irregular-Earth mixed-path model discussed in the next section.

### 3.1.3 The Irregular-Earth Mixed-Path Model

Irregularities in the terrain have a greater effect at higher frequencies, so an irregular terrain model is more appropriate when terrain irregularities become appreciable in size with respect to a wavelength. The smooth-Earth model is much more computationally efficient and many orders of magnitude faster than the irregular-Earth model, so in cases where the terrain is smooth enough, the smooth-Earth model can be used with minimal sacrifice in accuracy. Specific comparisons of smooth-Earth and irregular-Earth predictions with actual measurements have been made for different terrain irregularities [6].

For the MF band it was demonstrated that for terrain variations along the path of less than a wavelength, the smooth-Earth and irregular-Earth models were in close agreement. The irregular-Earth, mixed-path model in this ground-wave model uses an integral equation [33,34] to compute the propagation loss of a vertically polarized electromagnetic wave over irregular terrain. This approach is a point-to-point prediction method valid for frequencies between 10 kHz and 30 MHz. Later versions [33,34] of this model simulate terrain that is covered with forests, buildings, or snow, where the terrain cover is modeled as a slab of user-specified thickness, length, conductivity, and dielectric constant. Antenna heights of the transmitter and receiver antennas without a slab are included in the irregular-Earth propagation loss computations using the same height-gain functions as the smooth-Earth, mixed-path model. When a slab is included, a special height-gain function [33] is used for the antennas within or above the slab for the irregular-Earth mixed-path model.

The approach used by Ott [34] was to solve the irregular-Earth mixed-path model integral equation numerically using a technique based on Wagner's method [35]. The integral equation is a solution to a parabolic differential equation [34]. The complete derivation of the integral equation as well as the actual numerical evaluation of the integral equation can be found in the literature [36,37]. The parabolic wave equation can be derived from the general wave equation [34,36]. The general wave equation is given by:

$$\frac{\partial^2 \varphi}{\partial x^2} + \frac{\partial^2 \varphi}{\partial y^2} + k^2 \varphi = -2\pi\tau(x,y) \quad , y > y(x) \tag{37}$$

The solution to this equation satisfies an impedance boundary condition [36]:

$$\frac{\partial \varphi}{\partial n} = \frac{jk\Delta\varphi}{\sqrt{1+(y')^2}} \ , \ y=y(x), \ y' = \frac{dy}{dx} \tag{38}$$

where $\varphi$ is the vertical component of the electric field for vertical polarization or the vertical component of the magnetic field for horizontal polarization with time dependence $e^{j\omega t}$ [36]. The function $\tau(x,y)$ is the source distribution.

If we let $\varphi(x,y)=e^{-jkx}\psi(x,y)$, and substitute this into equation (37), then equation (37) is transformed into:

$$\frac{\partial^2 \psi}{\partial x^2} + \frac{\partial^2 \psi}{\partial y^2} - 2jk\frac{\partial \psi}{\partial x} = -2\pi\tau(x,y)e^{jkx} \tag{39}$$

If it is then assumed that the term $\partial^2\psi/\partial x^2$ is much smaller than the other terms in the equation, then the equation becomes:

$$\frac{\partial^2 \psi}{\partial y^2} - 2jk\frac{\partial \psi}{\partial x} = -2\pi\tau(x,y)e^{jkx} \tag{40}$$

This is a parabolic differential equation. The parabolic equation may be used to approximate the scalar wave equation if the polarization of the wave remains constant along the path and if the direction of propagation is at low angles and nearly horizontal [38]. The solution to this parabolic differential equation is an integral equation, where the path of integration is along the irregular ground on a line between the transmitter and the receiver. The integral equation has the form [34]:

$$f(x) = g(x,y)W(x,0) - \sqrt{j/x}\int_0^x f(\xi)e^{-k\phi(x,\xi)} \bullet$$
$$\left[y'(\xi)W(x,\xi) - \frac{y(x)-y(\xi)}{x-\xi} + (\Delta(\xi)-\Delta_r)W(x,\xi)\right] \bullet \sqrt{\frac{x}{\xi(x-\xi)}}\, d\xi \tag{39}$$

where $f(x)$ is the field normalized to twice the free-space field, and $\Delta_r$ is the normalized surface impedance at the transmitter antenna. The normalized surface impedance can be computed from $\sigma, \varepsilon$, and the frequency $f$ using the expressions given earlier in this paper in the smooth-Earth discussion. $\Delta(\xi)$ is a function of these parameters at the integration point on the path $\xi$, and $\Delta(\xi)-\Delta_r$ is zero for a homogeneous path. The surface impedance $\Delta(\xi)$ along the path can be continuous or have abrupt changes along the path.

$$W(x,\xi) = 1 - j\sqrt{\pi P}\; w(-\sqrt{u}) \tag{42}$$

$$P = -jk[\Delta(\xi)]^2 \frac{(x-\xi)}{2} \tag{43}$$

$$y'(\xi) = \frac{dy}{d\xi} \tag{44}$$

$$u = P\,[1 - \frac{y(x) - y(\xi)}{\Delta(x-\xi)}]^2 \qquad for\ \ \xi < x \tag{45}$$

$$\phi(x,\xi) = \frac{[y(x) - y(\xi)]^2}{2(x-\xi)} + \frac{y^2(\xi)}{2} - \frac{y^2(x)}{2} \tag{46}$$

$$w(-\sqrt{u}) = e^{-u}\mathrm{erfc}(j\sqrt{u}) \tag{47}$$

$$w(\sqrt{-u}) = \frac{1}{j\pi}\int_{-\infty}^{\infty} \frac{e^{-t^2}dt}{\sqrt{u}+t} \tag{48}$$

This integral definition of the complementary error function (equation 48) is defined in [21]. Figure 3 shows the geometry for the irregular-Earth mixed-path model. The symbol *x* denotes the distance from the transmitter antenna at which the receiver antenna is located, *y(x)* denotes the height of the receiver antenna with respect to the transmitter antenna height, $\xi$ is the distance of the integration point measured from the transmitter, *y( ξ)* denotes the height of the integration point with respect to the transmitter height, and *g(x,y)* is the antenna pattern factor for the transmitter antenna. The transmitter terrain is at zero height and serves as a reference height since all heights are used as program input only after the terrain height at the transmitter is subtracted from each terrain height.

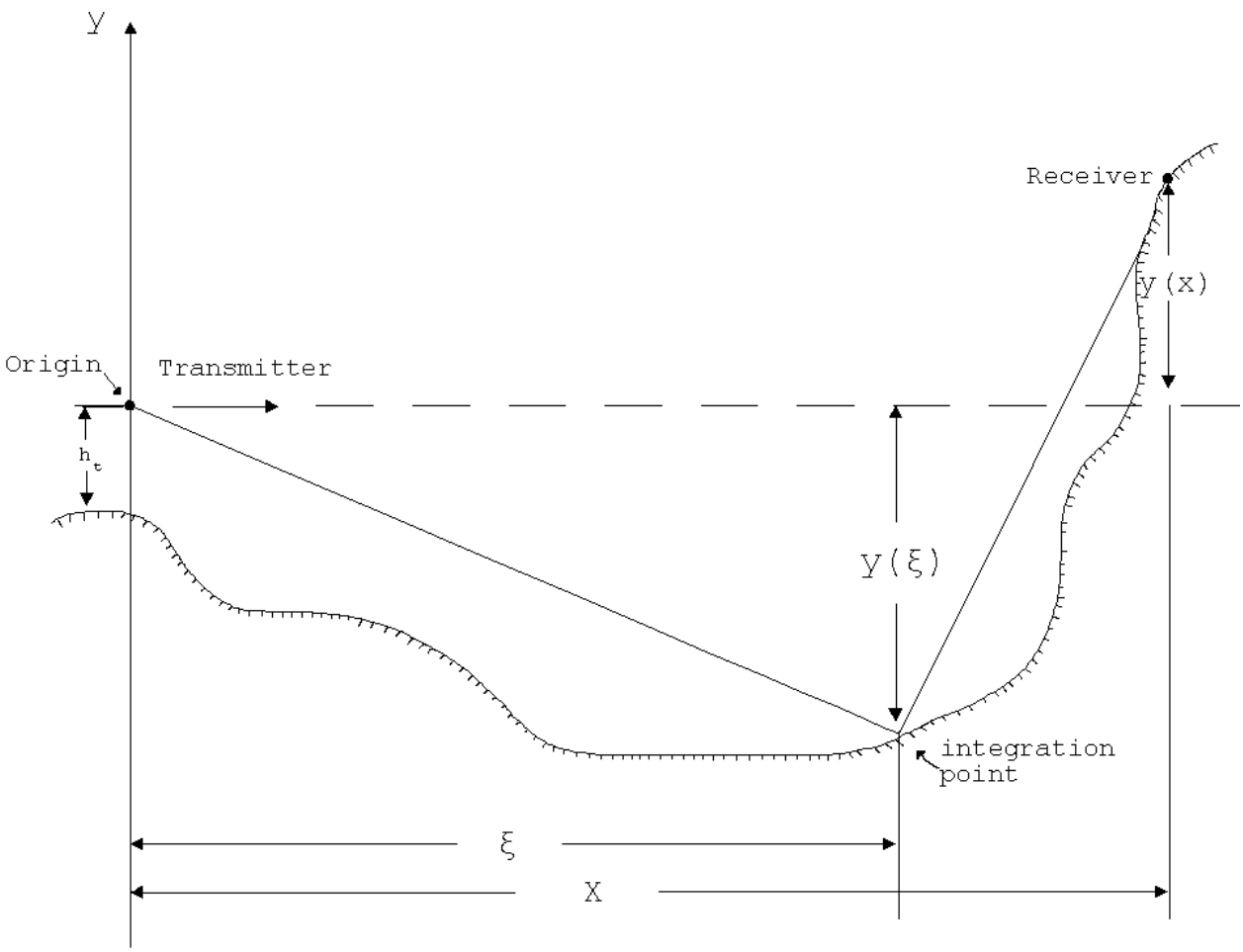



Figure 3. Geometry for integral equation irregular-Earth model along the great circle path.

*W( x,ξ)* is the flat-Earth attenuation function. The terms within the bracket under the integral sign represent the surface impedance, height, and slope of the ground at the integration point *ξ*. The integral equation computes the relative field *f(x)* at a point *x* along the path in terms of *f ( ξ)*, its value at all previous points along the path.

The numerical solution of the integral equation is obtained by dividing the path up into discrete intervals. The field *f(ξ)* must be known initially at a series of discrete points. The field at the very next point is determined by fitting a second order polynomial in each of the intervals and then performing a numerical integration. The initial points are determined using the Sommerfeld attenuation function, and then the integral term of the equation is evaluated. The computer program implementation calculates the electric field at all desired points between the transmitter and receiver. The integral is evaluated over the irregular ground between the terminals, and the ground is considered inhomogeneous in the direction of propagation along the path between the transmitter and receiver.

It has also been assumed that the electrical properties of the ground may be described by its surface impedance which is a function of the ground constants σ and ε. The integral equation method can be used with any variations of terrain represented as heights along the propagation path. The terrain heights can change abruptly or continuously. The terrain does not need to be described by standard geometrical features or canonical shapes. The terrain can be represented by a completely arbitrary profile. The program assumes that the terrain varies linearly between points input by the terrain file or user. If the program decides that it needs additional terrain points between those given, then linear interpolation is used to determine terrain heights between available terrain heights. The program automatically chooses the spacing so that the terrain is sampled frequently enough for an accurate representation of the terrain variation, and so that the numerical integration of the integral equation is sufficiently accurate, but a compromise is also made so as to prevent excessive computation time. The distance between points should be long so as to minimize computation time, since the computation time is proportional to the square of the number of computation points, but it should be short to accurately represent the terrain and provide an accurate numerical integration.

The analytical details of the integral equation and its derivation are described in the references [33,34]. In both of these references, good agreement is found between this method and other analytical computation methods. Comparisons of calculations with measurements have also been made [6,39,40]. It has been found that for terrain variations smaller than a wavelength, the smooth-Earth and smooth-Earth mixed-path models result in comparable accuracy to the irregular-Earth mixed-path model, so it may be more efficient to use one of the smooth-Earth models.

## 4. SKY-WAVE PROPAGATION

A medium frequency sky wave will be returned back to Earth by the ionosphere if the degree of ionization in the appropriate regions is sufficient to refract and reflect the incident electromagnetic wave. Ionospheric propagation models for medium frequencies can predict this degree of ionization in the different layers to determine the amount of signal that is refracted and reflected and hence the system performance. The two regions that are responsible for the refraction and reflection of medium frequencies are the D region and the E region. The first region encountered by the sky wave is the D region which extends in a layer that is 50 to 90 km above the Earth's surface [41,42]. It is a region of low electron density whose degree of ionization is determined primarily by solar photoionization. This region usually exists during the daytime. This region has a low electron density and the electrons collide with predominantly neutral gases, so this region absorbs the energy in the MF radio waves that pass through it during the daytime hours [41,42]. The MF sky wave is therefore highly attenuated as it passes through the D layer during the daytime.

At night in the absence of the photoionization created by the sunlight, the ionization in the D region is at a much lower level or is nonexistent, so the D region no longer absorbs the energy from the MF sky wave passing through it. The MF sky wave proceeds to the E region above this D region where it is reflected and refracted. The E-region ionization is from multiple sources that exist all of the time, so it is active during both the daytime and the nighttime. E-region ionization in the daytime

is predominantly caused by solar ultraviolet and x-rays, while E-region ionization at night is caused predominantly by cosmic rays and meteors. The E region occurs at heights of 90 to 140 km, and it attains its maximum electron density near 100 km [41,42]. This is the height within the E region that is the predominant reflecting medium for MF propagation at night. Since the sky wave at medium frequencies is strongly attenuated by the electron density in the daytime D region, long distance radio-wave propagation during the daytime is limited by how far the surface wave component of the ground wave can diffract around the Earth and its terrain features. Consequently, ionospheric radio-wave propagation at MF is practical only at night [41,42].

The sky wave can contribute to a desired signal and also generate undesirable interference to the desired signal depending on the distance between the transmitter and receiver. At night the undesirable interference from the sky wave can manifest itself as adjacent and co-channel interference to stations that it would not normally reach in the daytime. System performance for close and far distances between the transmitter and the receiver depend on the frequency and ground conductivity, since the magnitude of the ground wave is a function of these two parameters. The sky wave and the ground wave will add vectorially. At 0.5 MHz over average ground, the ground wave predominates over the sky wave from the transmitter site out to distances of about 150 km, where the two signals are equal. The signals add as vectors, and destructive and constructive interference can occur. At distances beyond 150 km the sky wave is the predominant signal. At a signal frequency of 1.5 MHz, the distance where the two signals are equal reduces to 45 km, because of the increased loss at the higher frequency. At even higher frequencies the attenuation losses of both the ground-wave and the sky-wave signal are greater, so the distance where the signal levels are equal in amplitude becomes smaller. If the transmitter and receiver are close to each other, the ground-wave signal is usually predominant over the sky-wave signal, and the ground-wave signal is normally considered the desired signal. For large separations, the sky-wave signal predominates and is the desired signal. In the region between close and far transmitter to receiver separations, either the sky-wave or ground-wave signal can interfere with the dominant signal and cause possible signal cancellation. The desired signal in many practical cases is the ground-wave signal.

The sky wave at AM broadcast frequencies can actually become stronger with increasing distance from the transmitter, because the sky wave that reaches the receiver represents energy radiated from increasingly lower elevation angles, and the characteristics of MF broadcast antennas in the elevation plane are such that the gain that launches or receives the sky wave increases in magnitude over the lower elevation angles as it passes through and goes beyond the main beam. Beyond this point the gain that launches the sky wave decreases as shown in Figure 4. Figure 4 is an elevation pattern for a quarter-wave monopole antenna that is typically used at a transmitter site.

The MF sky-wave model [7] predicts sky-wave propagation parameters using empirical formulas derived from measured data and assumes an undisturbed ionosphere. The propagation of the sky wave is latitude (actually geomagnetic latitude) dependent, but not all models include this effect. The field strength decreases with increasing latitude [47]. The amount of the decrease is proportional to the path length along which propagation takes place. The field strength can decrease as much as 10 dB with a 10 degree increase in latitude at large distances on the order of 4000 km

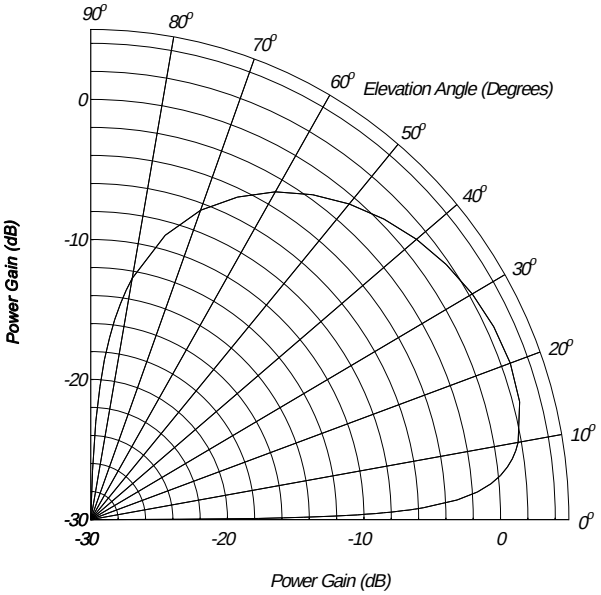



Figure 4. Elevation plane pattern for a quarter-wave monopole on a ground screen.

[43,47]. At 1000 km the decrease in field strength for a 10 degree increase in latitude is only 5 dB. Curves are available for field strengths at other distances and latitudes [47]. The sky-wave models that have latitude and path length dependence can predict the amount of decrease [43]. During fading the field strength amplitude follows a Rayleigh distribution [44] for latitudes less than 40 degrees. The propagation of the sky wave at MF is also dependent on distance, time of day, and frequency. The effects due to frequency are minor.

Semi-empirical algorithms have been produced for ionospheric radio-wave propagation. One such algorithm is that developed by the International Telecommunications Union (ITU) [43,46]. The ITU method is the only one that accounts for the variation of sky-wave propagation with frequency, but it has a frequency-dependent term that reduces the predicted field strength with increasing frequency. One reference, [47], notes that measurements in the United States show a frequency dependence that is exactly the opposite of what the ITU method predicts. The measurements show that signals measured at 1530 kHz at sunset or sunrise are about 15 dB greater than those at 700 kHz. This difference becomes smaller and smaller as the time of day approaches midnight and reduces to 3 to 5 dB at two hours after sunset or two hours before sunrise. The difference at midnight is negligible. Rather than adding the error that is incurred when using the ITU model [47], the effects of frequency for the sky wave are generally neglected. The frequency dependence over the range of 500 kHz to 1600 kHz is small, so it is often ignored and the field strength at 1000 kHz is taken as representative of the entire band [44].

Seasonal dependence has been demonstrated by measurements. The field strength received from a transmitter is at a minimum during the summer and reaches a maximum during spring and fall. The field strength decreases in the winter, but is not as low as the minimum achieved during the summer. The difference between the summer minimum and the spring/fall maximums is about 15 dB at 500 kHz and reduces to about 3 dB at 1700 kHz [44].

There are a number of sky-wave field-strength prediction methods in use. Three methods have been accepted for use in sky-wave propagation prediction: (1) the FCC/Region 2 method for computing sky-wave field strengths [45], (2) the ITU-R (formerly CCIR) recommended method [43,46], and (3) a procedure proposed by Wang [47] for use in the United States and Region 2. All of the procedures assume a reference field strength at 1 km from the transmitter in the development of their field strength curves (FCC Region 2 method) or field strength algorithms (ITU and Wang methods). Using the distance along the path plus other parameters that may be needed, such as frequency and geomagnetic latitude, the annual median field strength can be predicted. Some of the models do not use all of the parameters. This power is modified by the model using the actual transmitter power. The actual antenna gain in the elevation plane for the particular take-off angle needed to reach the reception area is factored in by the model. The take-off angles are also computed by the model using the geometry between the transmitter and receiver site. These methods are each described in more detail in the paragraphs that follow.

The FCC/Region 2 model is actually a combination of the FCC's curve of field strength versus distance for 50 percent of the time (for a year) for distances up to 4250 km, and the Region 2 expression for distances greater than 4250 km [7]. Measurements performed in 1935 were used by the FCC to generate the curve of field strength versus distance. The assumptions made during the development of this curve were that there is no dependency on frequency or latitude for the United States. The FCC considers this curve accurate for all frequencies and latitudes in the United States, but there is latitude dependence outside of the United States. The curve for field strength exceeded for 50 percent of the year is shown in Figure 5. From additional measurements performed from 1939 to 1944, the FCC determined that there is a dependence on latitude [7,48]. The new curves from those measurements can be used for interference analyses. The field strengths are further modified for each analysis by adjusting transmitter power and antenna gain. Because the curve only goes out to about 4250 km, the Region 2 algorithm is used beyond that distance [45]. The Region 2 algorithm is given by [45]:

$$F_c = \frac{231}{3 + \frac{d}{1000}} - 35.5 \qquad (49)$$

where $F_c$ is the characteristic field strength in dBuV/m, and $d$ is the distance in km. This expression is adapted from the results of long-distance measurements made in the late 1930s across the Atlantic and from North to South America. They are referred to as the ITU Cairo curves [47]. The field strength that is exceeded 10 percent (upper decile value) of the time is found by adding 8 dB to the

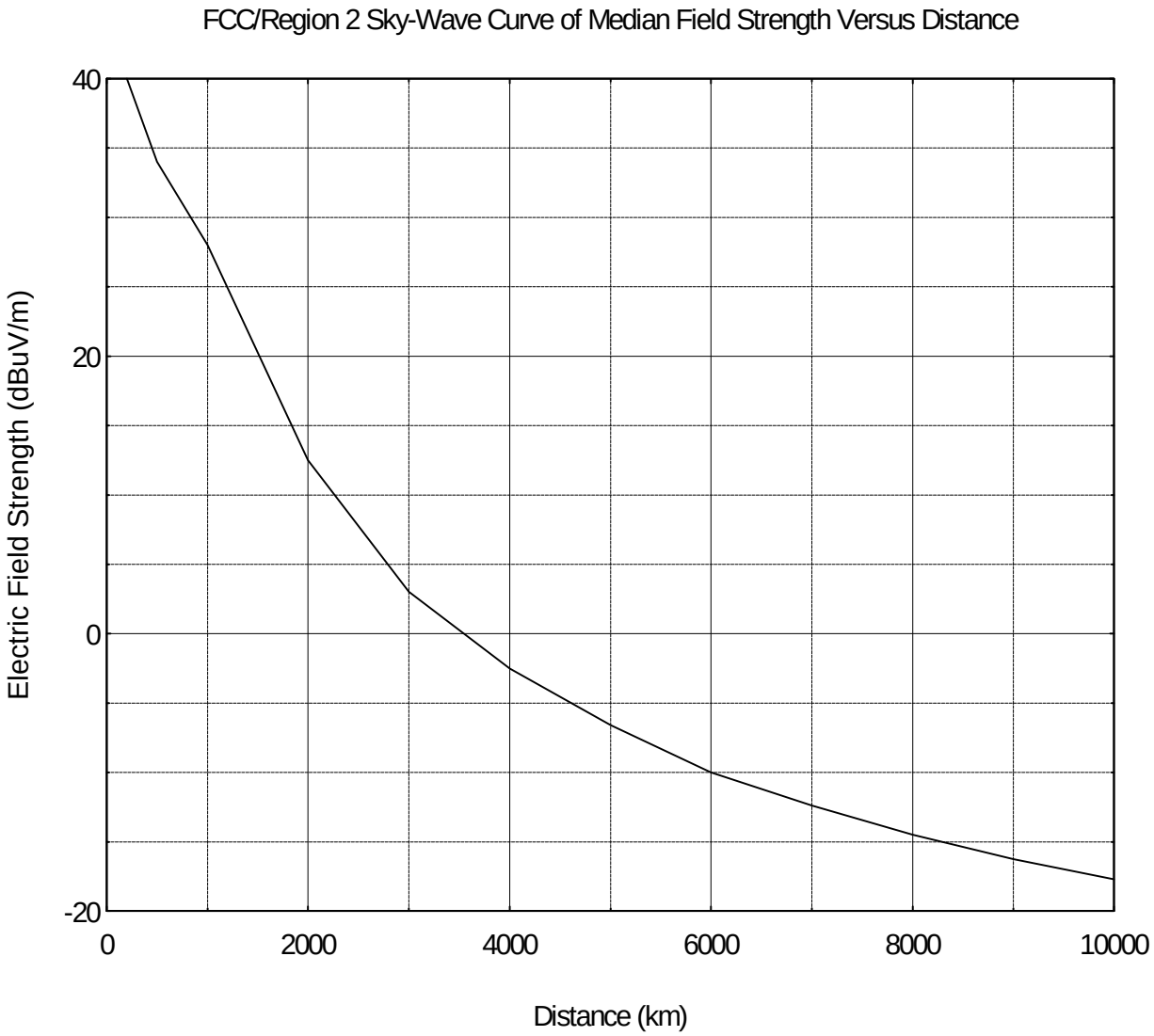



Figure 5. FCC/Region 2 sky-wave curve of median field strength versus distance.

median value of field strength versus distance [47]. The entire curve of field strength exceeded for 50 percent of the time versus distance for the combined FCC and Region 2 methods is shown in Figure 5.

The development of the ITU sky-wave field strength prediction method is a result of many modifications made since the 1930s [47,48]. These modifications were a result of knowledge gained from the measurements. The current ITU method uses the USSR method with certain modifications (such as the United Kingdom sea-gain correction) [7,48]. The expression [7,43] for field strength of the sky wave is:

$$F = V + G_s - L_p + 106.6 - 2\sin(\phi) - 20\log(p_s) - 0.001(K_r)(p_s) - L_t \quad (50)$$

where $F$ is the field strength in dBuV/m, $V$ is the transmitter cymomotive force above the reference 300 V in dB, $G_s$ is the sea-gain correction in dB, $L_p$ is the excess polarization-coupling loss in dB (defined graphically in ITU Recommendation 435-7 [43]), $\phi$ is the average of the transmitter and receiver geomagnetic latitudes, $p_s$ is the slant-propagation distance in km, $L_t$ is the hourly loss factor in dB, and $K_r$ is the loss factor in dB including ionospheric absorption, frequency, focusing and terminal losses, and losses between hops.

$$K_r = K + 0.01 b_{sa} R \quad (51)$$

where $R$ is the twelve-month smoothed international relative sunspot number, $b_{sa}$ is the solar activity factor ($b_{sa}$=0 for LF band; $b_{sa}$=4 for MF band for North American paths, 1 for Europe and Australia, and 0 elsewhere). For paths where the terminals are in different regions use the average value of $b_{sa}$ (ITU Recommendation 435-7) [43].

$$K = 3.2 + 0.19 f^{0.4} \tan^2[\phi + 3] \quad (52)$$

where $f$ is the frequency in kHz, and $\phi$ is the average geomagnetic latitude defined previously. For $\phi > 60$ degrees evaluate expression at $\phi = 60$ degrees. For $\phi < -60$ degrees evaluate expression at $\phi = -60$ degrees. For paths shorter than 3,000 km, $\phi = 0.5(\phi_T + \phi_R)$ where $\phi_T$ and $\phi_R$ are the latitudes at the transmitter and receiver respectively. The value of $L_t$ is nearly 0 dB for the time period from 4 hours after sunset to 2 hours before sunrise, so this term is ignored for nighttime propagation predictions.

During the daytime, 30 dB is subtracted from the nighttime field-strength prediction or added to the sky-wave loss prediction for the value of $L_t$(dB). A transition period occurs immediately after sunset and lasts till approximately four hours after sunset, and another occurs during the period from 2 hours before sunrise until sunrise where the field strength goes through this 30 dB change with a very steep slope. The shapes of the curves are not symmetrical for the transition from day-to-night and night-to-day [49].

The D layer of the ionosphere is characterized as having a strong dependence on frequency, but this is present only during the daytime. The E layer is the dominant contributor to LF and MF propagation at night and is only mildly dependent on frequency, so the effects of frequency of this layer can be neglected for most practical purposes [49].

For long distance paths (1000 to 6000 km), when the path is over sea or at least one end of the link is located on or near the seacoast, the phenomenon of sea gain can add from 3 to 10 dB to the predicted field strength [7,43]. However, a knowledge of the land-sea boundary information is necessary to assess the sea-gain phenomena. The sea-gain correction is normally set to 0 dB without this knowledge.

The ITU method makes predictions that depend on both frequency and geomagnetic latitude. The field strength values are not symmetrical about the geomagnetic latitude equal to 0 degrees. A family of field strength curves for 1000 kHz is shown in Figure 6. The ITU notes that this field strength expression predicts lower field strength values as the frequency is increased in the MF band [43], but measurements performed in the United States show that the field strengths are higher at the higher frequencies in the MF band when compared to those measurements at the lower frequencies. Because of this discrepancy, the ITU method has not found wide acceptance as a worldwide prediction method. Davies [43] also refers to measurements and gives an equation that is a function of frequency. He recommends the use of predictions at 1000 kHz to represent the entire MF band.

In an effort to create a valid model that would give reasonably accurate predictions in Region 2, Wang [47] developed an MF sky-wave model after examining all of the available MF methods. The original FCC curves have a hump at roughly 100 km which Wang concluded was due to ground-wave interference present in the 1935 data. The curves become smoother and better behaved after removal of these data points. The Wang expression for field strength is:

$$F_c = 95 - 20\log(d) - [\,6.28 + 4.95\tan^2(\phi_m)]\sqrt{\frac{d}{1000}} \qquad (53)$$

where $F_c$ is the characteristic field strength in dBuV/m referenced to 100 mV/m at 1 km, $d$ is the distance in km, $\phi_m$ = geomagnetic latitude of the midpoint of the path in degrees.

Wang recommends that if $d$ is less than 250 km, then the expression should be evaluated at 250 km. There are also limits that the latitude, $\phi_m$, be less than or equal to +60 degrees, and greater than -60 degrees. When compared to the ITU expression, Wang's expression is symmetrical about zero degrees latitude and is not dependent on frequency. Figure 7 shows a family of field strength curves for several values of $\phi_m$.

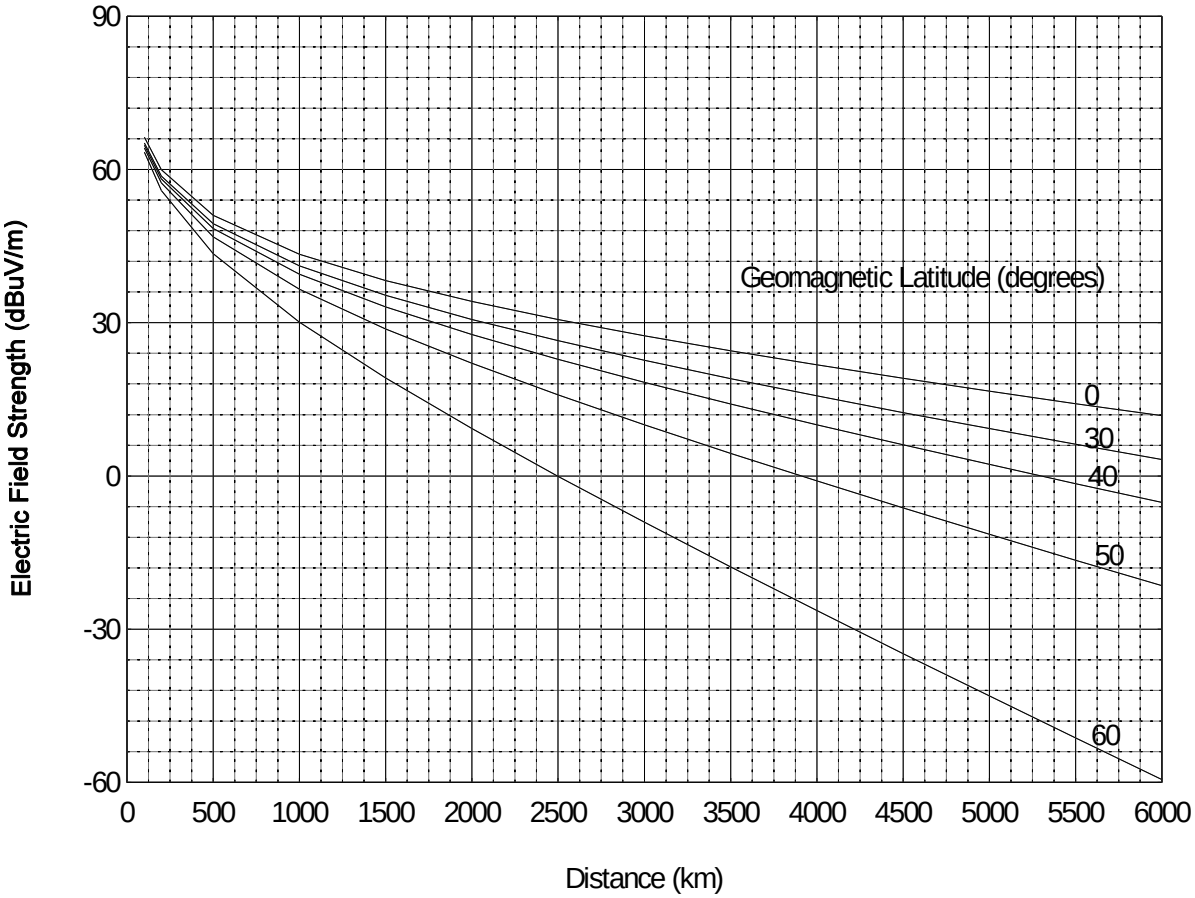



Figure 6. ITU sky-wave curves of median field strength for several values of geomagnetic latitude at 1000 kHz.

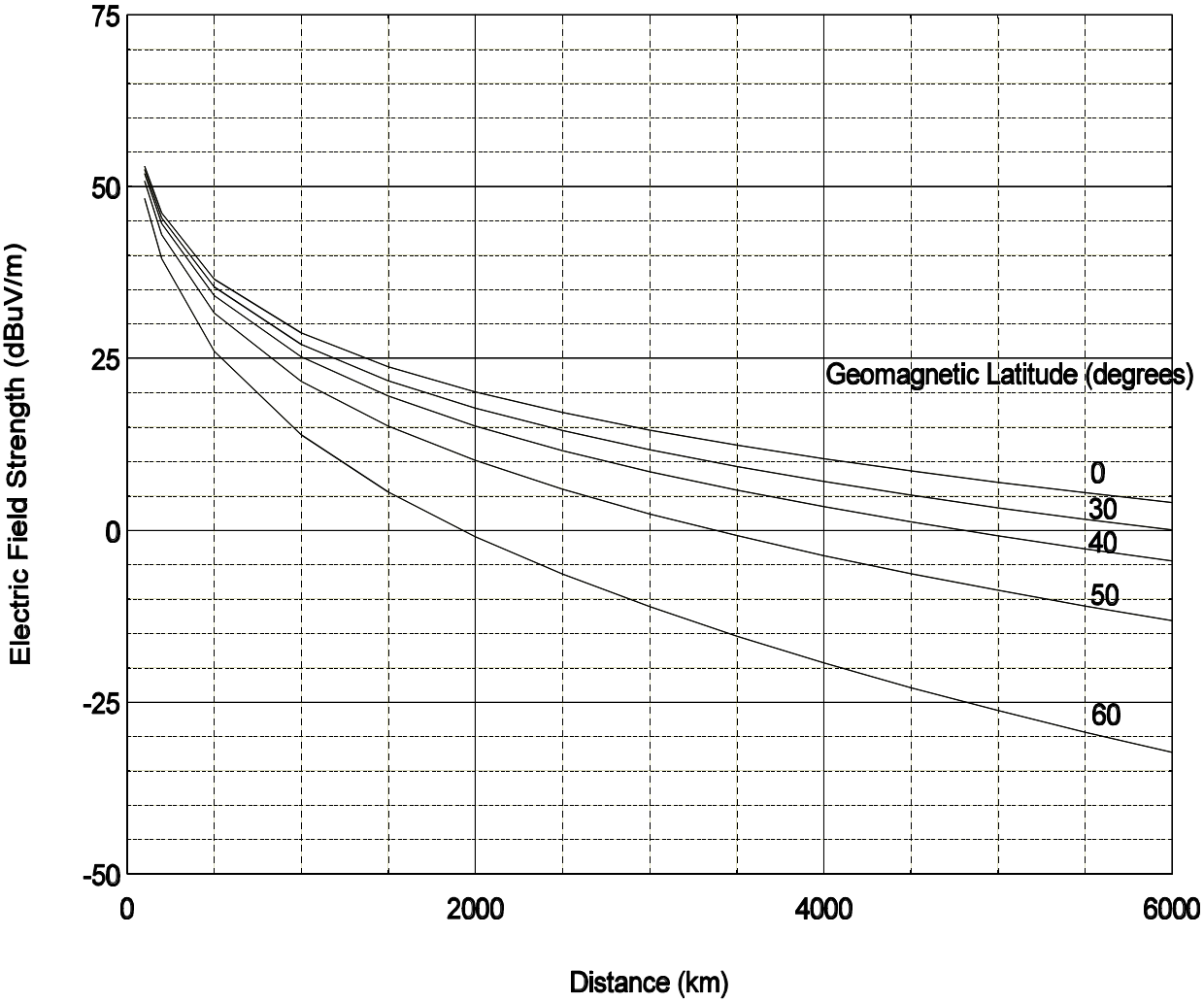



Figure 7. Wang sky-wave curves of median field strength for several values of geomagnetic latitude.

## 5. ANTENNA MODELING

Accurate antenna modeling is necessary to determine the elevation and azimuth gain variability for prediction of the actual gain to be used in launching the sky wave at the appropriate take-off angles, and the ground-wave gain at the horizon angle. The performance of an antenna on or near the surface of the Earth is very dependent on the interaction with the lossy Earth. This is especially true for antennas at MF. Currently available techniques for analyzing antennas over ground with computer algorithms are time consuming and require conversion or normalization for use in system computations. This process will be described in this section. The gain of the antenna is a function of the antenna geometry, materials used, ground conductivity, ground dielectric constant, frequency, elevation angle, and azimuth angle. The gain required for systems performance analysis is usually calculated with respect to an isotropic radiator in free space or some other reference antenna such as a dipole. Conventional methods such as free space analysis could not be used due to the close proximity of the antennas to a lossy Earth. Antenna modeling techniques at medium frequencies must account for the actual gain that launches the ground wave. The end result for the antenna gain described in this paper has been transformed to be referenced to an isotropic radiator in free space.

There are several methods for modeling antennas that are in close proximity to a lossy Earth. Some of these are not valid for an antenna located right on the surface and require that the antenna be 0.2 wavelengths above the surface or the algorithm used in the calculation will not be valid. These algorithms that assume free-space conditions or negligible ground effects should not be used to model antennas that are too close to the Earth, because the results are poor. The model selected for analyzing antennas makes use of extensive method-of moments calculations and is implemented in a computer program titled the Numerical Electromagnetics Code (NEC) [50]. It is an accurate method for analyzing antennas at these low and medium frequencies where the antennas are small or comparable to a wavelength in size. Numerical methods are required to solve this problem and NEC is a good algorithm to use. The NEC program operates using a computation mode that implements a Sommerfeld integral computation for the determination of electromagnetic fields for antenna structures that are buried or penetrate the ground-air interface. This computation technique includes the reflected field below the interface, the field transmitted across the interface, and the fields above the ground-air interface. The algorithms used are also valid for antennas very close to the interface. The NEC program can also model near fields of the antenna very close to the antenna structure, in addition to being able to model the far field and compute antenna gain.

A different antenna gain phenomenon occurs with antennas at medium frequencies as compared to antennas at VHF, UHF and higher frequencies. The antenna principles are the same, but the surface wave becomes more signficant at MF. This is important because it is the surface wave that accounts for practically all of the energy transmitted and received at these frequencies. The concepts of gain and efficiency for antennas close to the surface of the Earth at MF are difficult to comprehend, since a major portion of the power launched by the antenna is absorbed by the lossy Earth. The electric field propagating along the surface of the Earth decreases faster than the usual reciprocal of the distance decay rate. In order to see this phenomenon, it is necessary to examine the Norton expressions [10] for the electric field resulting from an electric dipole above the surface of a finitely conducting Earth. Norton [10] in his effort to simplify the expressions developed by Sommerfeld

[13] came up with equations that clearly show the surface wave and space wave components. Jordan [54] deleted the higher order terms that are inversely proportional to the distance terms of Norton's equations for the vertical and radial directed components of the electric field in cylindrical coordinates. These higher order terms represent the induction and near field of the antenna and diminish in amplitude rapidly with distance. Jordan [54] further reduced the equation complexity by vectorially combining the equations for the vertical and radial directed field components, and then separating the resulting equation into a total space and total surface wave component. The resulting equations are:

$$E_{space} = j30IkL\left(\frac{e^{-jkR_1}}{R_1} + R_v\frac{e^{-jkR_2}}{R_2}\right)\cos\theta \tag{54}$$

$$E_{surface} = j30IkL(1-R_v)A(\rho)\frac{e^{-jkR_2}}{R_2}\sqrt{1-2u^2+u^2\cos^2\theta(1+\sin^2\theta/2)^2} \tag{55}$$

where $k=2\pi/\lambda$ as defined previously, $A(\rho)$ is the flat-Earth attenuation function defined previously, $I$ is the peak dipole current amplitude in amperes, $L$ is the length of the dipole in meters, $R_1$ is the distance between the dipole and the observation point in meters, $R_2$ is the distance between the dipole image and the observation point in meters, $R_v$ is the complex reflection coefficient for vertical polarization, $u^2=(\varepsilon_r+j\sigma/\omega\varepsilon_0)^{-1}$, and $\theta$ is the angle representing the direction of the incident wave measured with respect to the Earth's surface.

The equations (54 and 55) for the electric-field components of the space wave and the surface wave are plotted in Figure 8 for conditions representing MF frequencies with average ground. Examination of an electric-field strength pattern such as that displayed in Figure 8 shows that the electric field due to the space-wave pattern indicates a very small component at the horizon, but this is not what launches the surface wave component of the ground wave. The actual gain that launches the surface wave can be determined from a numerical electromagnetic approach by analyzing the specific antenna geometry. The normal pattern shown in Figure 8 as a dotted line is the electric-field antenna pattern responsible for launching the space-wave component of the ground wave consisting of the direct and reflected ground wave. This is equation (54). It is also responsible for launching the sky wave. The amplitude of the space-wave electric field decreases with distance and is proportional to the reciprocal of the distance. The electric-field pattern that launches the surface wave is shown as a solid line in Figure 8. This is equation (55). It is a plot of the unattenuated surface wave with $A(\rho)=1$ and represents the surface wave close to the antenna. For large numerical distances, the amplitude of the surface-wave electric field decreases as the reciprocal of the square of the distance. Notice that it has a maximum level at the surface and decreases rapidly with increasing elevation angle. For larger elevation angles greater than a few degrees the space wave

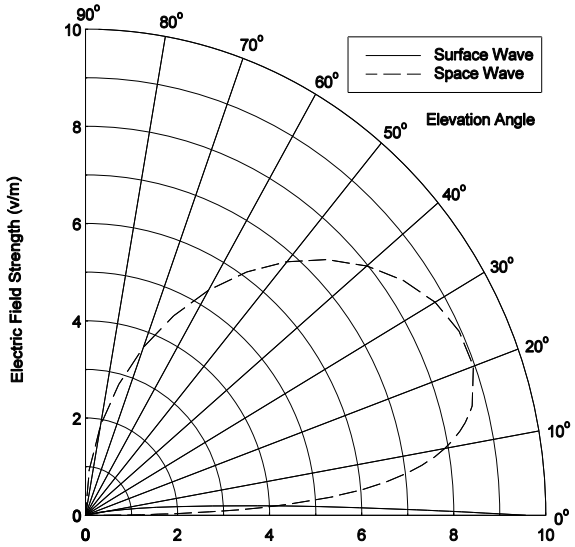



Figure 8. Space wave and unattenuated surface wave components of the ground wave for a vertical dipole at the Earth's surface for average ground conditions at 760 kHz.

contribution becomes more significant and is responsible for the launching of the space wave component of the ground wave and the sky wave. The relative geometry between most transmitters and receivers used for propagating ground-wave signals at MF frequencies will be at very low elevation angles with respect to each other. These elevation angles are on the order of one degree or less. The ground wave for these conditions will consist predominantly of the surface wave with little contribution by the space wave. Correct performance predictions will be obtained only when using this unique electric-field pattern that launches the surface wave to calculate an equivalent gain that correctly represents the magnitude of electromagnetic energy transmission or reception. Both the surface wave and the space wave components are included to represent the total electric field of a dipole or any antenna near a lossy Earth. As one or both antennas are raised in height a distance comparable to a wavelength above the Earth's surface, the surface wave becomes less significant and eventually negligible.

Receiver antennas at MF tend to be small in physical size with respect to a wavelength, and therefore have very low gains due to radiation efficiency considerations. The transmit antennas are usually more efficient since they are comparable to a wavelength in size. The antenna algorithm used to predict the antenna gain for low and medium frequency antennas computes an equivalent gain and represents the effectiveness of the antenna in launching or receiving the surface wave component of a ground wave. The gains for these antennas were derived from behavior analysis of extensive method-of-moments calculations using the Numerical Electromagnetics Code [50,51].

A short dipole was selected as a reference antenna due to simplicity of analysis and convenience in measurement. Many loss calculations in ground-wave analysis are referenced to short dipoles or monopoles. The computer program NEC is used to determine the equivalent gain of a short dipole over a lossy Earth with respect to an isotropic radiator in free space for the appropriate ground conductivities, ground dielectric constants, and frequencies. The relative performance of the subject antenna with respect to the short dipole is then determined using the NEC program. These two factors are then combined to obtain the equivalent gain with respect to an isotropic radiator in free space.

The gain of a short dipole antenna at the surface of a lossy Earth referenced to an isotropic radiator in free space can be derived from some basic relationships. The power density in free space for an isotropic radiator is given by Norton [52,53]:

$$\frac{e^2}{\eta} = \frac{P_r}{4\pi D^2} \tag{56}$$

where $e(V/m)$ is the electric field strength in volts per meter, $\eta\,(ohms)$ is the impedance of free space ($120\pi$ ohms), $D(m)$ is the distance from the antenna in meters, and $P_r(W)$ is the radiated power in watts.

Taking the square root of both sides and rearranging terms, the primary electric field strength from an isotropic antenna is:

$$e(V/m) = \frac{\sqrt{30P_r(W)}}{D(m)} \tag{57}$$

The primary electric field strength from any antenna in free space is:

$$e(V/m) = \frac{\sqrt{30P(W)g}}{D(m)} \tag{58}$$

where $g$ is the equivalent antenna gain ratio referenced to an isotropic radiator in free space and $P$ is the transmitter input power in watts. If the units are changed the above equation becomes:

$$e(mV/m) = 173\frac{\sqrt{P(kW)g}}{d(km)} \tag{59}$$

where $e(mV/m)$ is the electric field strength in millivolts per meter, $P(kW)$ is the transmitter power in kilowatts, and $d(km)$ is the distance in kilometers.

If the antenna is a short vertical dipole element ($g$=3) at but not touching the surface of a perfectly conducting Earth, then:

$$e(mV/m) = 300\frac{\sqrt{P(kW)}}{d(km)} \tag{60}$$

This is the familiar 300 mV/m at one km for a radiated power of one kW over a perfectly conducting Earth.

The electric field strength for a lossy Earth and an arbitrary gain $g$ is given by Terman [8] as:

$$e(mV/m) = 173 \bullet A \bullet \frac{\sqrt{P(kW)g}}{d(km)} \tag{61}$$

where $A$ is the Norton approximation [9] to the Sommerfeld attenuation function [13]. This attenuation function was described previously in the discussion on ground-wave propagation. If this expression is rearranged to solve for $g$ and the logarithm of both sides is taken, the gain of a short dipole antenna at but not touching the surface of a lossy Earth referenced to an isotropic radiator in free space is:

:

$$G_d(dB) = 10 \bullet \log\left[\frac{e^2(mV/m)d^2(km)}{(173)^2 P(kW)A^2}\right] \tag{62}$$

The effectiveness of an antenna in launching a surface wave which will be referred to as "equivalent gain," is then determined by first calculating a ratio called the relative communication efficiency for the antenna as a function of the ground constants, frequency, antenna geometry, and azimuthal direction. The relative communication efficiency in decibels ($dB$) is then added to the reference dipole gain. The relative communication efficiency ($RCE$) [53] of an antenna is defined by:

$$RCE(dB) = 10 \bullet \log\frac{(E_t)^2 P_r}{(E_r)^2 P_t} \tag{63}$$

where $E_r(V/m)$ is the electric field strength predicted by NEC at reference distance $d$ and input power $P_r$ for a short dipole, $P_r$ ($W$) is the dipole antenna input power from NEC used to compute $E_r$ ($V/m$), $E_t$ ($V/m$) is the electric field strength predicted by NEC at reference distance $d$ and input power $P_t$ for the subject antenna, and $P_t$ ($W$) is the subject antenna input power from NEC used to compute $E_t$.

The "equivalent gain" $G_a(dBi)$ of the subject antenna over lossy Earth referenced to an isotropic radiator in free space is given by:

$$G_a(dBi) = G_d(dBi) + RCE(dB) \tag{64}$$

The "equivalent gain" referenced to an isotropic radiator in free space can now be used for communication system analysis. The result is a term similar to power gain that can be defined in the presence of a lossy Earth. A number of antennas were modeled using this technique.

One antenna that was modeled for the DGPS correction signal at 300 kHz consisted of a top-loaded monopole on a ground screen. This antenna is typical of a DGPS antenna that was installed at a site in Appleton, Washington. This site is one of the first installation sites for the DGPS system. DGPS signals radiated from this antenna site were measured extensively [55]. The monopole antenna is a tapered triangular shaped steel tower consisting of steel tubing 1.52 cm in diameter. The monopole length is 91.16 meters which is only 0.0912 wavelength at 300 kHz. The cross section of the monopole is an equilateral triangle measuring 0.61 meters on a side for most of its length and is tapered to a point on each end. There is a copper radial wire ground screen with 120 radials of 0.32 cm diameter that are each 100 meters in length. There are also twelve copper top-loading elements approximately 138 meters in length symmetrically located around the monopole extending from the top of the monopole down to the ground just outside but not touching the edge of the radial wire ground screen. The top-loading elements are 0.95 cm in diameter. Their purpose is to increase the efficiency of the antenna. The antenna is omnidirectional in the azimuth plane. The elevation plane

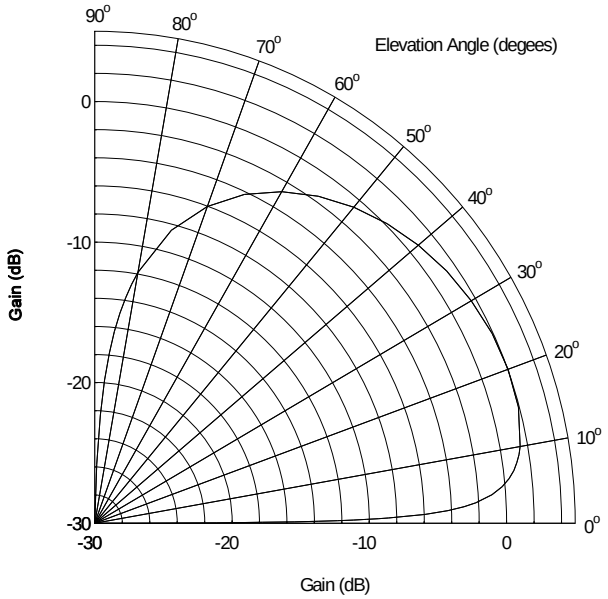



Figure 9. Elevation plane pattern for the space wave antenna power gain for the DGPS transmitter site antenna for average ground conditions at 300 kHz.

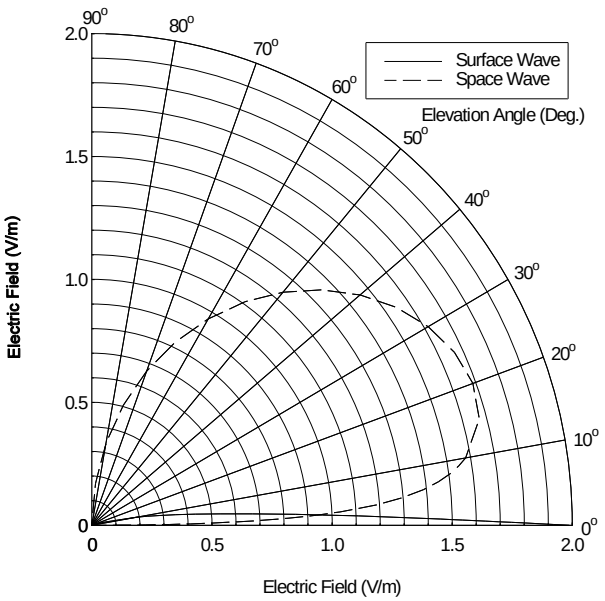



Figure 10. Electric field strength antenna patterns of the space wave and the surface wave for the DGPS transmitter site for average ground conditions at 300 kHz.

pattern for the space wave antenna power gain is shown in Figure 9. Notice the amplitude of the space wave pattern at the horizon. Figure 10 shows antenna patterns in terms of electric field strength for both the space wave and the surface wave for this antenna. The equivalent gain for launching the surface wave component was determined to be 3.2 dBi using the technique described previously, which includes the efficiency factor of 53 percent (-2.75 dB). This antenna gain occurs in all azimuth directions since the antenna is symmetrical in all azimuth planes. This equivalent antenna gain occurs at an elevation angle of zero degrees, and rapidly decreases in amplitude with increasing elevation angle. The loss due to impedance mismatch was assumed to be negligible, since the voltage standing wave ratio (VSWR) was less than 1.5:1. This antenna gain computation was verified by measurement of field strength from the actual DGPS site that uses this antenna [55].

Reception characteristics of a 300 kHz signal from a one meter antenna mounted on a van test vehicle were also determined using the equivalent gain technique. A short whip (one meter in length) on a van test vehicle was modeled to determine the antenna gains to use for system performance calculations. These gains will be much lower than what may be expected for this type of antenna due to the inefficient operation of small (with respect to a wavelength) vehicle antennas. Antennas were modeled at 300 kHz for DGPS and 760 kHz for the AM subcarrier ATIS. The antennas are much shorter than a wavelength and can also suffer from impedance mismatch loss into the receiver. Since the van test vehicle was also much smaller than a wavelength, it was found to have a negligible effect on the antenna as expected. The model for the van consisted of closely spaced metal wires that represented the geometry of the metal surface of the entire test van. There is only a slight pattern asymmetry of a few tenths of a dB created by the van asymmetry. Figure 11

shows the power gain pattern in the elevation plane for the space wave for the one meter whip at 300 kHz mounted in the center of the van roof. Notice the gain amplitude in comparison to Figure 9, even though the patterns have the same general shape. The equivalent gain for launching the surface wave was calculated for this antenna to be -21.3 dB. This gain exists in all azimuth directions since the antenna is symmetrical in this plane. The elevation angle for this equivalent gain is zero degrees

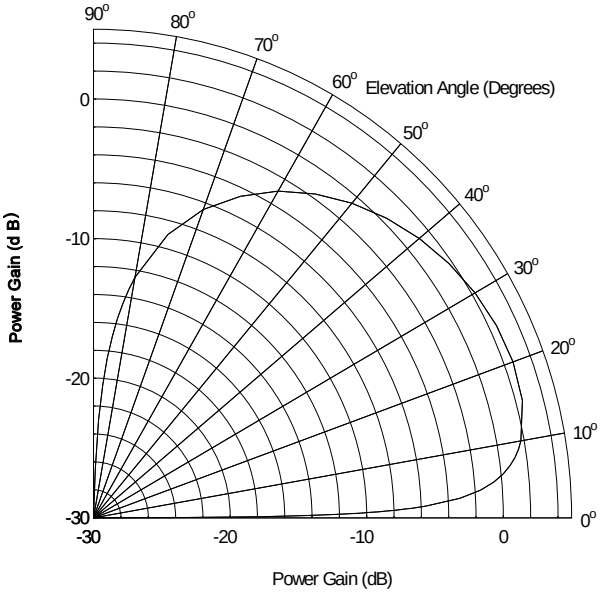



Figure 11. Power gain antenna pattern in the elevation plane for the space wave for the DGPS one meter whip mounted in the center of the van roof for average ground conditions at 300 kHz.

(the horizon). The power gain in the elevation plane of the antenna pattern for the same one meter antenna on the van roof at 760 kHz is shown in Figure 12. The equivalent gain for launching the surface wave was calculated to be -13.1 dB. The impedance mismatch loss can add a significant amount of loss to the antenna gain if the antenna is severely mismatched. If the characteristics of the receiver impedance and the cabling between the receiver and the antenna are known, then the mismatch loss can be calculated and included in the calculation of gain. An impedance mismatch characterized by a VSWR of less than 1.5:1 has been measured, so the impedance mismatch loss for this case is negligible.

A single quarter-wavelength monopole on a large ground screen (120 radials each $\lambda/4$ in length) was also modeled to simulate a broadcast transmitter for an AM radio station at 760 kHz. The monopole has a symmetrical pattern in azimuth. The resulting power gain pattern in the elevation plane at any azimuth angle is shown in Figure 13. The equivalent gain that launches the surface wave was determined to be 4.7 dB for this antenna.

A more complex antenna was also modeled. This antenna is a model of the actual antenna used at station KTLK at 760 kHz in Denver, Colorado. Two configurations are used: one for nighttime

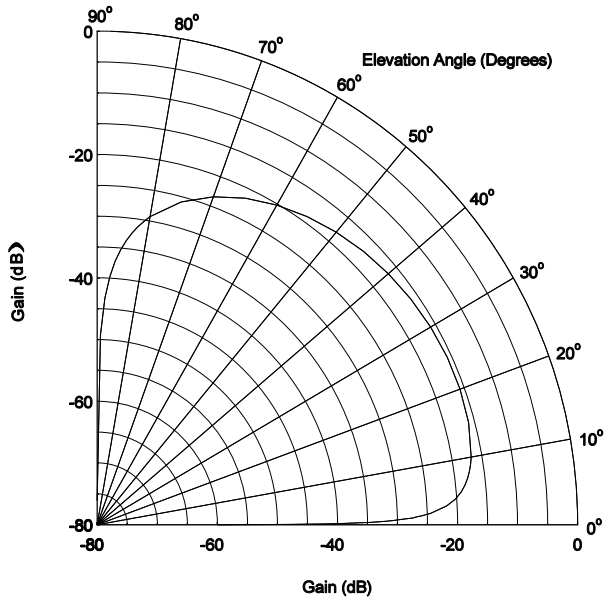



Figure 12. Power gain antenna pattern in the elevation plane for the space wave for the one meter whip antenna mounted in the center of the van roof for average ground conditions at 760 kHz.

operation, and one for daytime operation. The nighttime configuration consists of four monopole towers arranged in a physical array with the geometry and electrical phasing given in Table 2. All antenna tower positions and phasing are relative to tower 1. The azimuth pattern is shown in Figure 14. This pattern is at an elevation angle of zero degrees and represents an equivalent gain that launches a surface wave. It is not the space wave pattern which would have a very low gain at this elevation angle of zero degrees. The daytime configuration consists of two monopole towers arranged in the geometry and phasing given in Table 2. The azimuth pattern is shown in Figure 15. This pattern for the daytime antenna configuration is also the equivalent gain that launches the surface wave.

Figure 16 shows an elevation cut on the azimuth beam maximum at an azimuth angle of 225 degrees for the nighttime KTLK antenna configuration. Figure 17 shows an elevation cut on the beam maximum at an azimuth angle of 195 degrees for the daytime KTLK antenna. Figures 16 and 17 are elevation cuts of conventional antenna patterns of power gain showing the small magnitude of the gain at the horizon and for small elevation angles.

Table 2. Geometry and Phasing for Station KTLK Daytime and Nightime Antenna Arrays.

**Daytime Antenna Array**

| Tower | Field Ratio | Phase (deg) | Spacing (deg) | Bearing (deg) | Height (deg) |
|---|---|---|---|---|---|
| 1 | 1.000 | 360.0 | 00.0 | 00.0 | 89.0 |
| 2 | 1.350 | 451.0 | 134.8 | 116.5 | 89.0 |

**Nighttime Antenna Array**

| Tower | Field Ratio | Phase (deg) | Spacing (deg) | Bearing (deg) | Height (deg) |
|---|---|---|---|---|---|
| 1 | 1.000 | 360.0 | 00.0 | 00.0 | 89.0 |
| 2 | 0.980 | 462.0 | 90.0 | 75.0 | 89.0 |
| 3 | 0.800 | 272.0 | 134.8 | 116.5 | 89.0 |
| 4 | 0.820 | 530.0 | 90.0 | 158.0 | 89.0 |

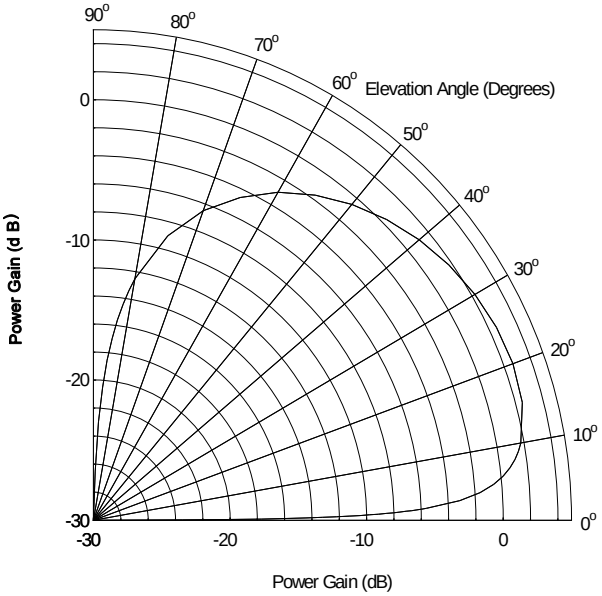



Figure 13. Power gain antenna pattern in the elevation plane for a quarter-wave monopole antenna on a ground screen for average ground conditions at 760 kHz.

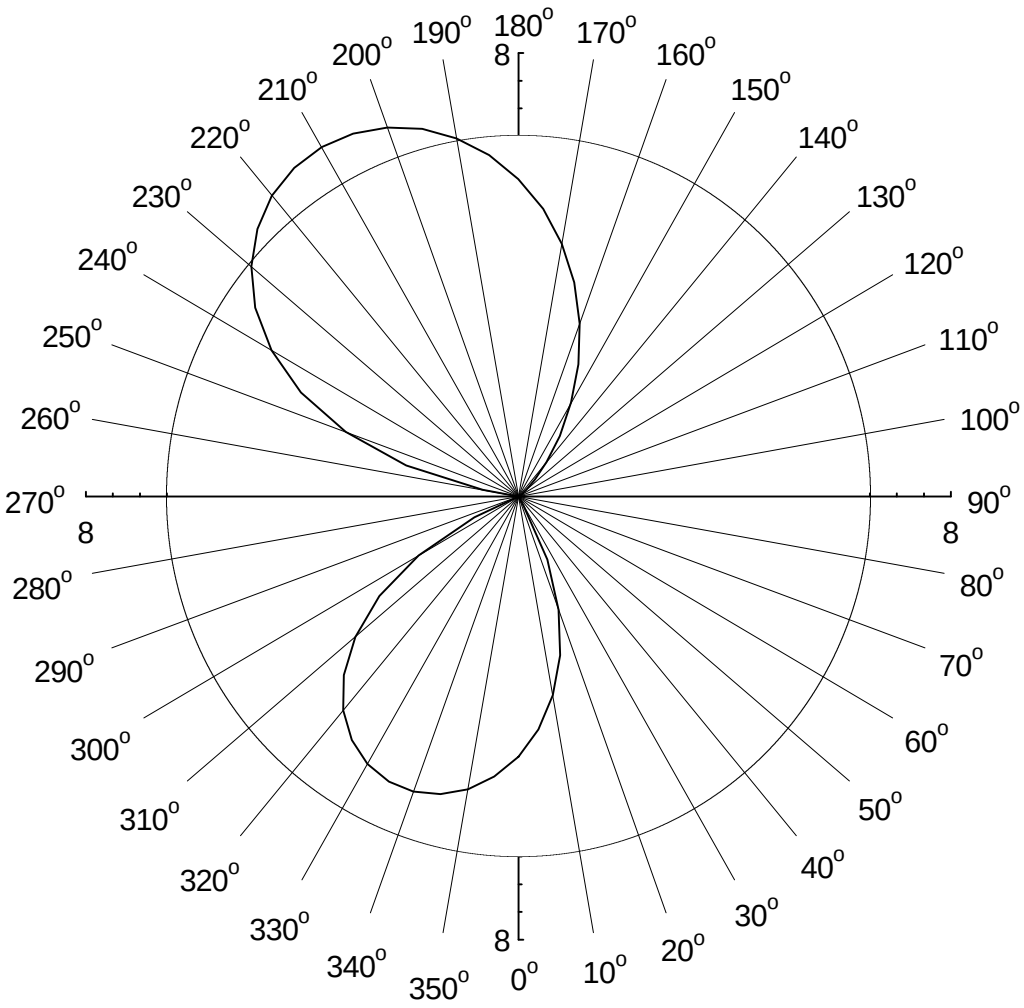
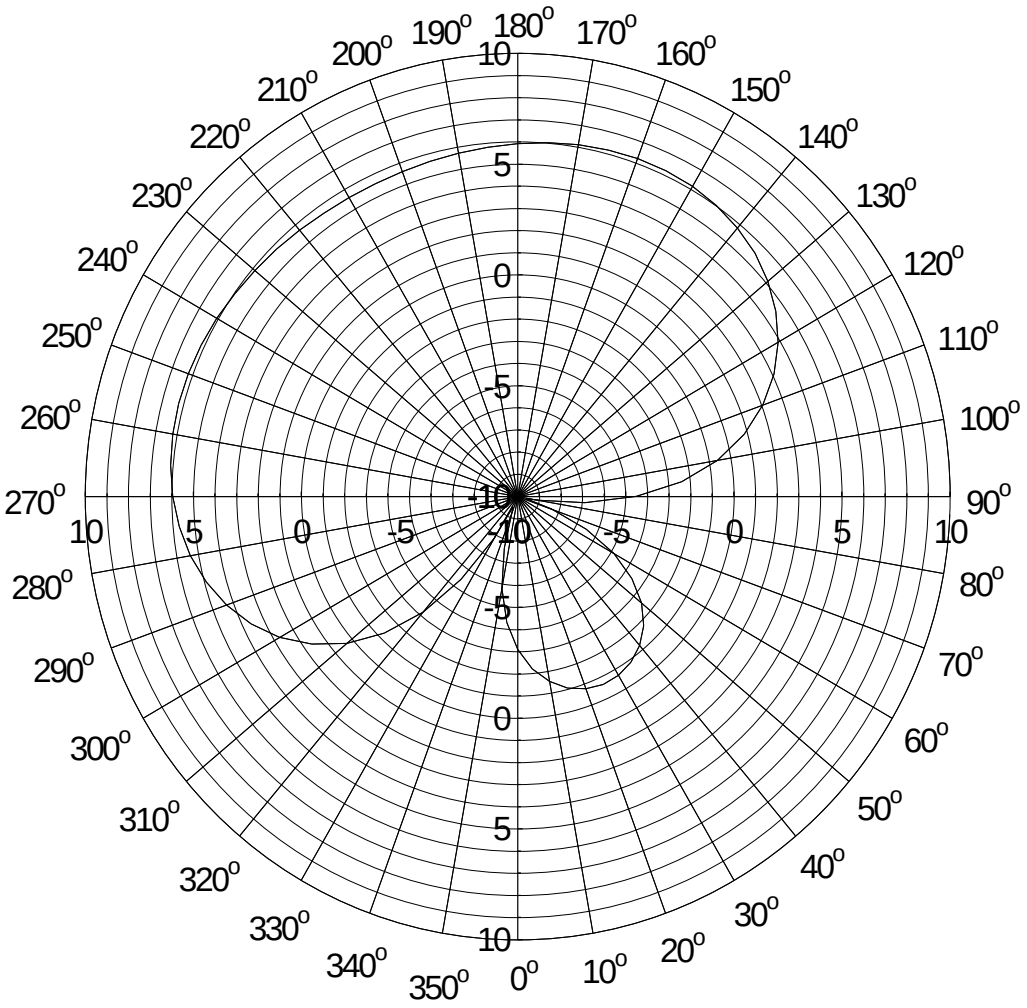



Figure 14. Equivalent gain antenna pattern for station KTLK nighttime antenna configuration versus azimuth angle for average ground conditions at 760 kHz.




Radial Scale is in dBi

Figure 15. Equivalent gain antenna pattern for station KTLK daytime antenna versus azimuth angle for average ground conditions at 760 kHz.

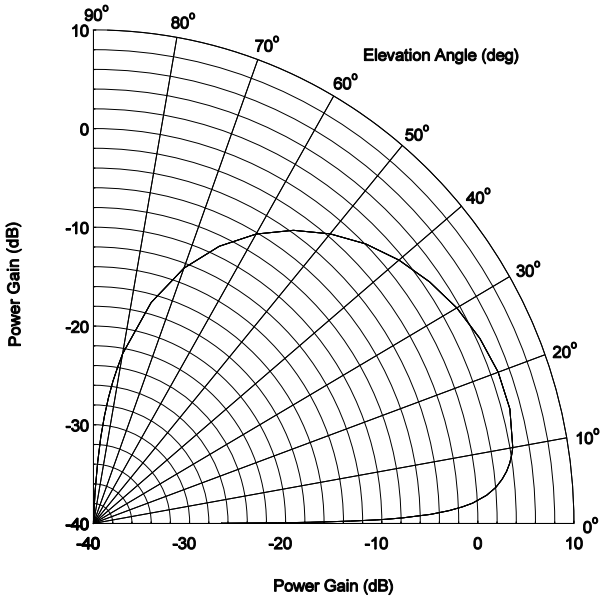



Figure 16. Power gain antenna pattern in the elevation plane on azimuth beam maximum for the KTLK nighttime antenna for average ground conditions at 760 kHz.

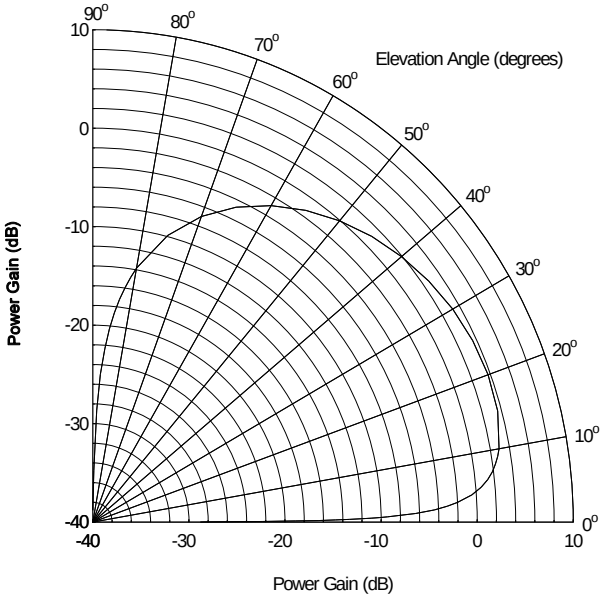



Figure 17. Power gain antenna pattern in the elevation plane on azimuth beam maximum for the KTLK daytime antenna for average ground conditions at 760 kHz.

## 6. SYSTEM PERFORMANCE CALCULATIONS AND PREDICTIONS

System performance calculations can be made using the propagation models described previously in this paper. Antenna gains for the system performance predictions are factored in to represent the actual gains of these antennas. The final calculations take into account the antenna gains of the transmitter antenna at the transmitter site and the receiver antenna at the receiver site or test vehicle. In some systems analysis applications, it is necessary to calculate electric field strength near a receiver antenna knowing the received power level into a spectrum analyzer. When using a spectrum analyzer or receiver, correction must be made to the received power levels to calculate electric field strength in the vicinity of the receiver antenna, since most coverage calculations are in field strength.

The equation to calculate electric field strength, E(dBuV/m) from received power is [16]:

$$E(dBuV/m) = P_r(dBm) + 77.21 + 20\log f(MHz) - G_r(dBi) + L_c(dB) \qquad (65)$$

where $P_r(dBm)$ is the received signal power which is referenced at the output of the antenna terminals but by appropriate adjustment of the losses can be moved to the reference point of the input to the spectrum analyzer or receiver, $f(MHz)$ is the frequency in MHz, $G_r(dBi)$ is the gain of the receiver antenna, and $L_c(dB)$ is the loss in the cable.

The receiver antenna gain in this expression must also be corrected to account for the degradation in gain as a function of elevation angle for receiving a surface wave, sky wave, or space wave shown previously in Figure 4. The line-of-sight from the receiver to the transmitter antenna is typically at (depending on distance from the transmitter and receiver, and transmitter and receiver antenna heights above mean sea level) an elevation angle of less than a few degrees. Over this range of elevation angles the gain of the receiver antenna for a sky wave can vary from 10 to 20 dB or more below the main beam gain. The peak gain of this antenna is small due to the low antenna efficiency at these frequencies. This additional reduction in antenna gain due to elevation angle increases the electric field strength required for system operation, which is proportional to the decrease in antenna gain in decibels. This can be seen from equation (65) above.

The gain for launching and receiving a ground wave is calculated using the NEC code mentioned earlier and converting the computations in the output to an equivalent gain referenced to an isotropic radiator. The gain and pattern for launching and receiving a sky wave can also be computed using NEC directly, since it computes a space wave antenna pattern in addition to the specific information needed to obtain the ground-wave equivalent gain. The results of these calculations were shown in the previous section.

Once confidence is obtained in the prediction algorithms for antenna models, then predictions of area coverage of a station can be performed. Figures 18 and 19 show KTLK station coverage computed from the ITS model [7] for the daytime coverages for both smooth-Earth and smooth-Earth mixed-path propagation models. The differences in the two figures are a result of considering a mixed path.

The borders for the states of Colorado, Wyoming, and Nebraska are shown. Figures 20 and 21 show station coverage computed from the ITS model [7] for the nighttime coverages for both smooth-Earth and smooth-Earth mixed-path propagation models. The electric-field strength values are given in units of dB microvolts per meter (*dBuV/m*). They illustrate the difference in coverages when the mixed-path data are taken into consideration. The prediction with the smooth-Earth mixed-path model shows greater coverage near the station where the ground wave propagation predominates. The ground constants were taken from the data base contained in the LF/MF model [7]. The ground constants and the mixed path only affect the ground wave propagation, but station KTLK uses different antenna configurations for daytime and nighttime, which also affects antenna performance and coverage area. The transmitter power also changes from 1kW at night to 50 kW during the daytime. The nighttime antenna configuration was specifically designed to mininize the chance for interference at night to an adjacent or cochannel station northeast of station KTLK, because the sky wave makes it possible to propagate appreciable level signals at very long distances. The antenna array configurations for station KTLK were described in Table 2 previously. The patterns in these coverage plots are different than those in the actual antenna pattern predictions of Figures 14 and 15, because Figures 14 and 15 are equivalent gain antenna patterns for launching the surface wave described previously. Figures 20 and 21 were created by the model using a composite of the equivalent gain antenna patterns for the surface wave and the space wave antenna patterns for the skywave. The resulting combination will look different than the spatial gain distribution of the individual antenna patterns.

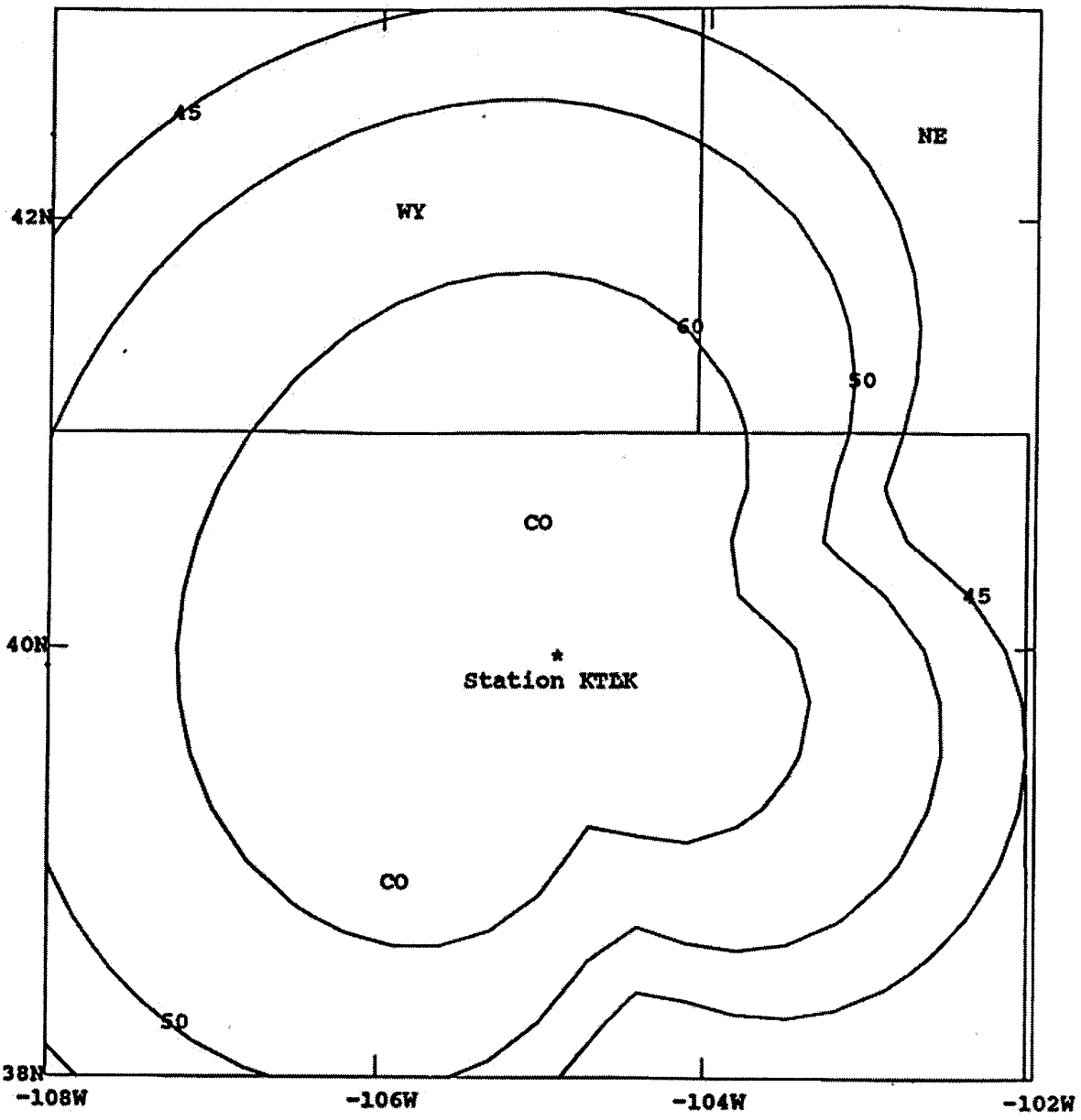



Figure 18. Predicted KTLK day coverage contours (dBuV/m) using the smooth-Earth model.

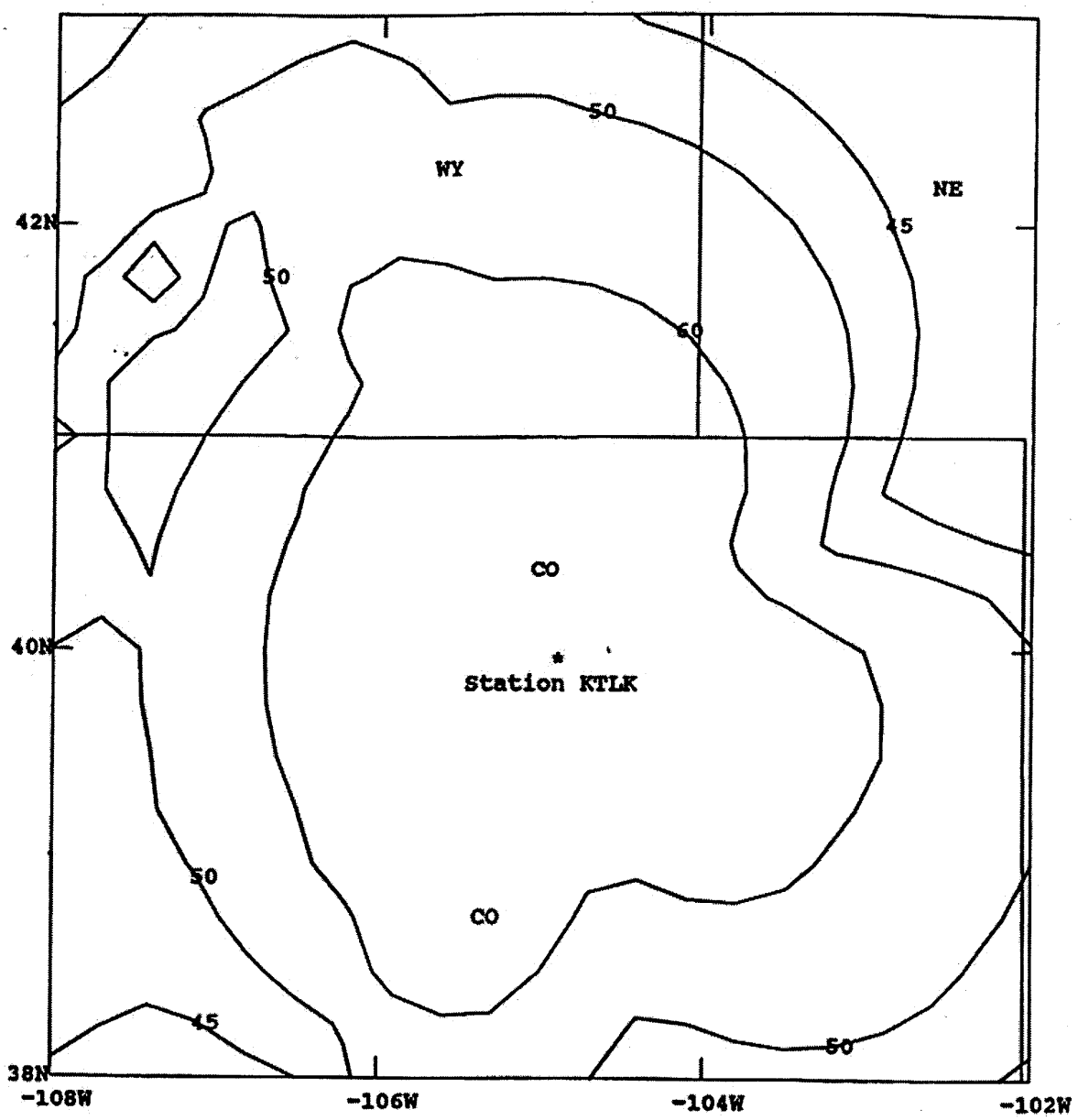



Figure 19. Predicted KTLK day coverage contours (dBuV/m) using the smooth-Earth mixed-path model.

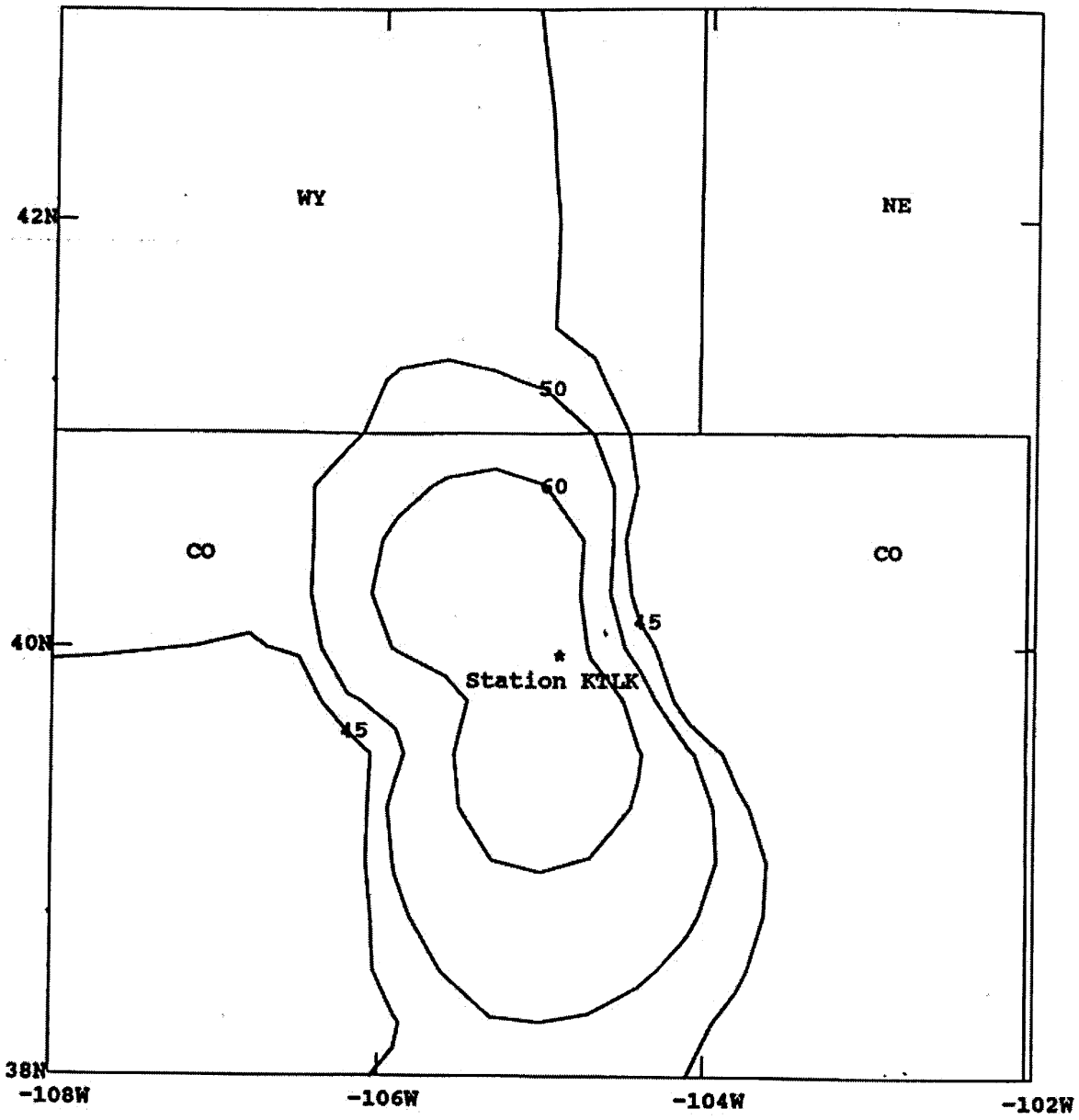



Figure 20. Predicted KTLK night coverage contours (dBuV/m) using the smooth-Earth model.

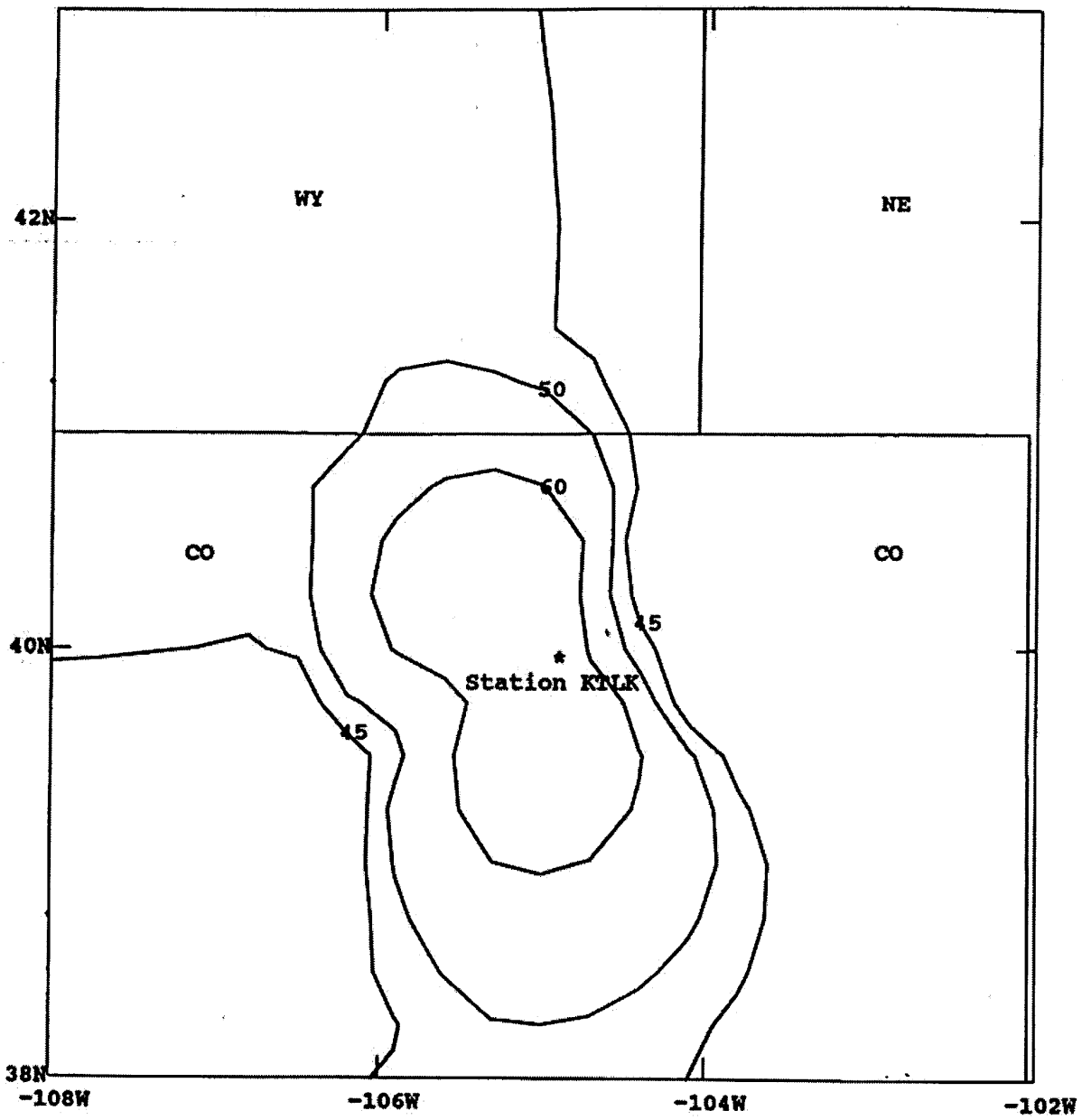



Figure 21. Predicted night coverage contours (dBuV/m) using the smooth-Earth mixed-path model.

The data used to plot Figures 22 and 23 were taken from the ITS model [7] using the point-to-point computation mode for the nighttime antenna configuration for the smooth-Earth and smooth-Earth mixed-path propagation models. Both figures are for a particular radial 330 degrees wrt due North for a long range nighttime prediction that includes both the ground-wave and the sky-wave components. The propagation model factors in the appropriate gains from the receiver and transmitter input geometry. The appropriate height-gain functions are also factored in to take into account nonzero antenna heights at both the transmitter and receiver locations. The combination of

the ground-wave and sky-wave propagation models also has an effect on the coverage, so the contours will look different than the spatial gain distribution of the antenna patterns. Both the ground wave and sky wave are plotted separately. When the sky-wave and ground-wave magnitudes become comparable to each other, they can combine constructively or destructively to either vectorially add together or produce a null at that particular distance from the station. The ground wave is a deterministic phenomenon, but the sky wave is a stochastic phenomenon, so the combination of the two is a stochastic process that will vary with time as ionospheric conditions vary. The smooth-Earth ground-wave model and the sky-wave model are equal at 170 km in Figure 22, but the smooth-Earth mixed-path ground-wave model in Figure 23 predicts that the ground wave and sky wave are equal at 190 km. The smooth-Earth mixed-path model is generally more accurate, since it takes into account the presence of a mixed-path ground constant condition if the data base of ground constants shows that it exists. The smooth-Earth model assumes a homogeneous Earth with one pair of values for the ground constants over the entire path.

System performance computations were made for several examples where measured data were available. Data were available from the DGPS site at Appleton [55,56]. Figure 24 compares the results of performance prediction calculations with the measured data for the Appleton, WA to Pendleton, WA path. The measured data for the Appleton site were obtained from reference [55]. The equivalent gain technique was used to determine antenna gains for system calibration. Figure 25 is a plot of the terrain contour over the Appleton to Pendleton path. The nulls of Figure 24 appear to correspond to when the measurement vehicle was located in deep canyons and behind large terrain peaks. Other extensive data were available for demonstrating agreement between predictions and measurements at various sites in the continental United States in the DGPS band of 285 to 325 kHz [56]. The reference [56] describes the results of comparisons of actual measurements to predictions over many paths. This DGPS signal is used for differential position correction of the GPS signal.

An extensive measurement program was performed at medium frequencies [40]. Figures 26 and 27 compare the measured data from two of the data runs at Canyonlands, Utah along a 45 km path from this reference with the model predictions. Data [40] were available from two medium frequency signals both at 520 kHz and 1618 kHz. There is good agreement between measurements and predictions. The irregular-Earth mixed-path model in the LF/MF model was used to perform the predictions, since the terrain is considered rough in comparison to a wavelength as shown in Figure 28. A smooth-Earth or smooth-Earth mixed-path prediction would not be accurate for this computation, since the terrain variations are large with respect to a wavelength. This reasoning was described earlier in the section on ground-wave propagation.

Propagation modeling and systems analysis can be used to resolve and explain actual measurements. An example of this can be demonstrated with recent measurements. A measurement was performed in Boulder, CO to determine the nighttime and daytime electric field strength received from the Appleton, WA DGPS site at 300 kHz (private communication J.R. Hoffman, February 8, 1999).

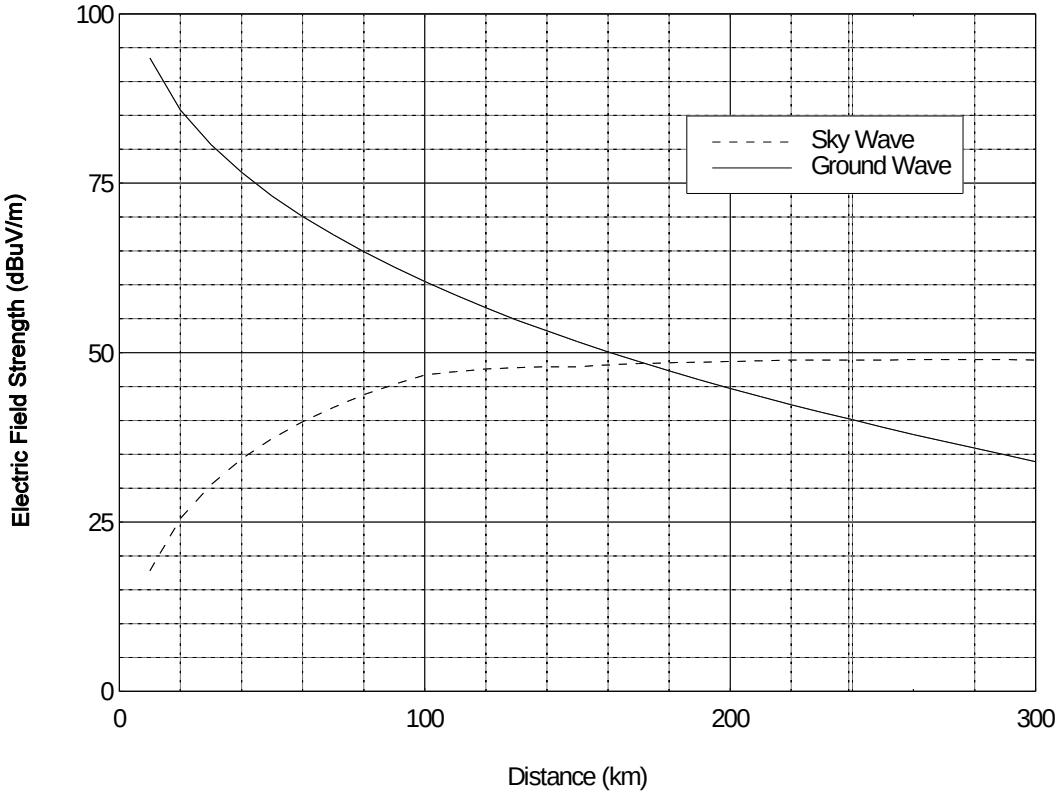



Figure 22. Electric field strength vs distance from station KTLK at nighttime on 330 degree radial using the smooth-Earth model.

Nighttime measurements of electric field strength consistently averaged 30 dBuV/m over several days with good quality DGPS messages. This is in good agreement with model predictions using the LF/MF model [7]. These results are shown in Figure 29 where contours of electric field strength from the Appleton DGPS site are plotted over a map of the Northwestern United States. Daytime measurements of 14 dBuV/m were also measured over several days, but there were no successful DGPS messages, since the signal levels from the Appleton DGPS site were too low. Predictions of electric field strength from the Appleton DGPS site resulted in -10 dBuV/m levels. This result is shown in Figure 30.

After searching a database of signals at this frequency, three other sites were found at 300 kHz. The LF/MF model was used to predict the daytime levels of electric-field strength from these sites. Two of these sites, one in Spearfish, SD and the other in Auburn, NE, were found to be capable of generating electric-field strengths at levels of 10 to 15 dBuV/m in the Boulder, CO area. Even though these two sites were at the same frequency, no successful DGPS messages were decoded since they were a different type of beacon site and were due to Federal Aviation Administration (FAA) beacons radiating at 300 kHZ. The propagation model was able to account for the levels of electric field strength at 300 kHz in Boulder, CO that were measured.

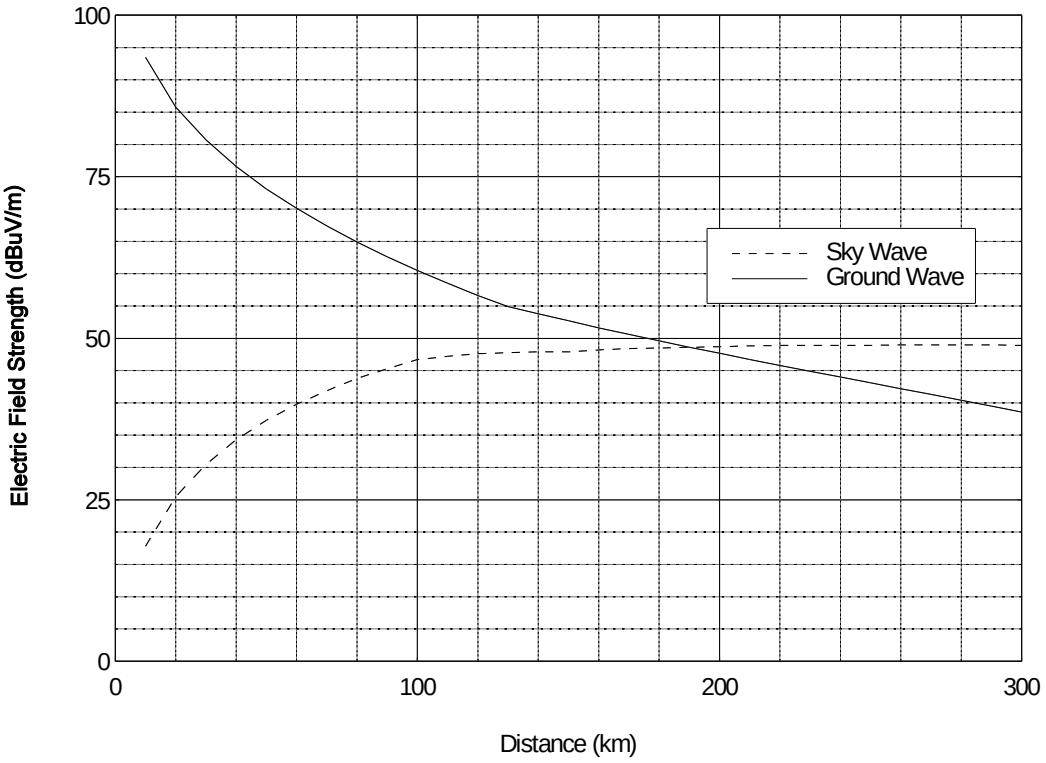



Figure 23. Electric field strength vs distance from station KTLK at nighttime on 330 degree radial using the smooth-Earth mixed-path model.

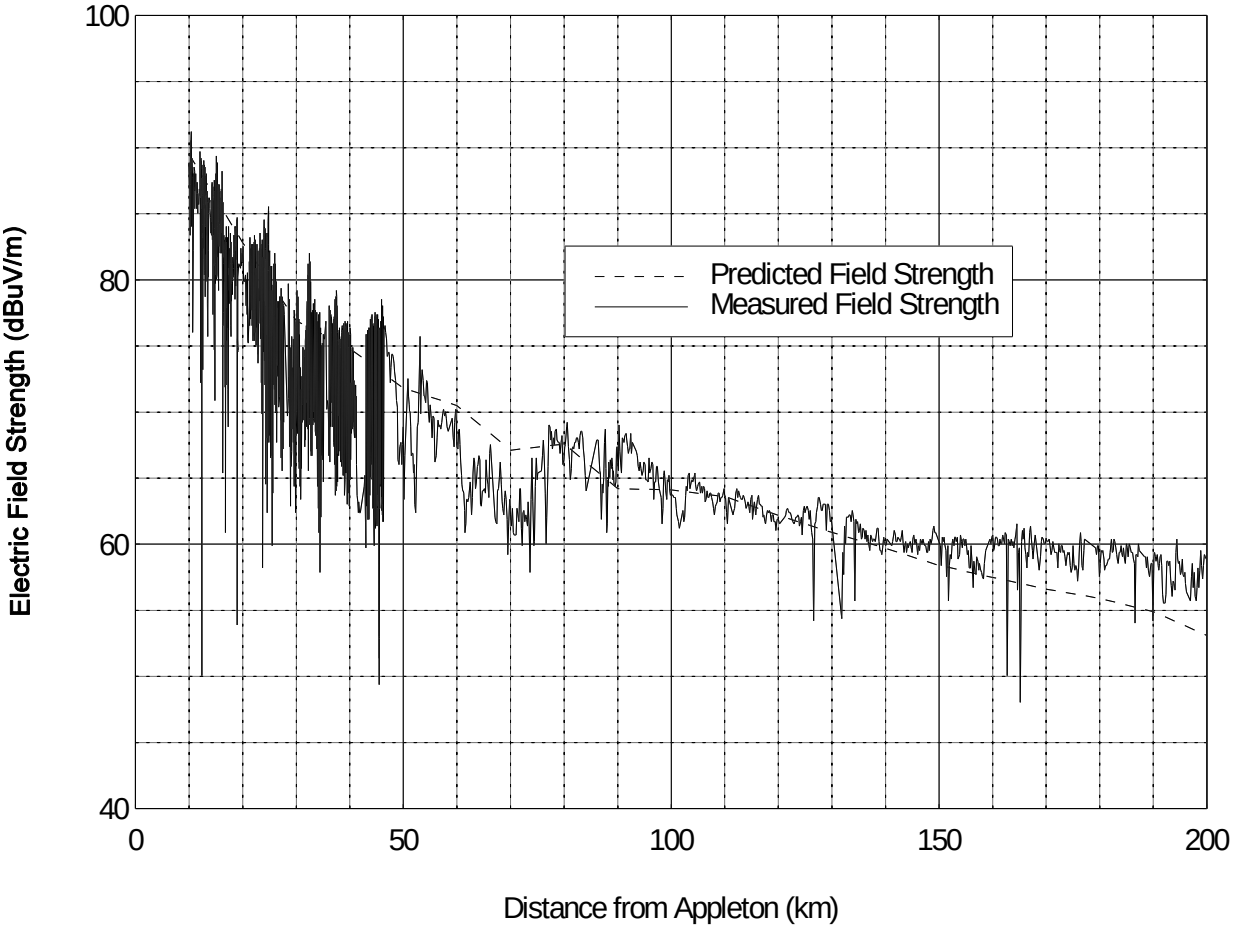



Figure 24. Comparison of measured and predicted DGPS field strength for the Appleton to Pendleton path.

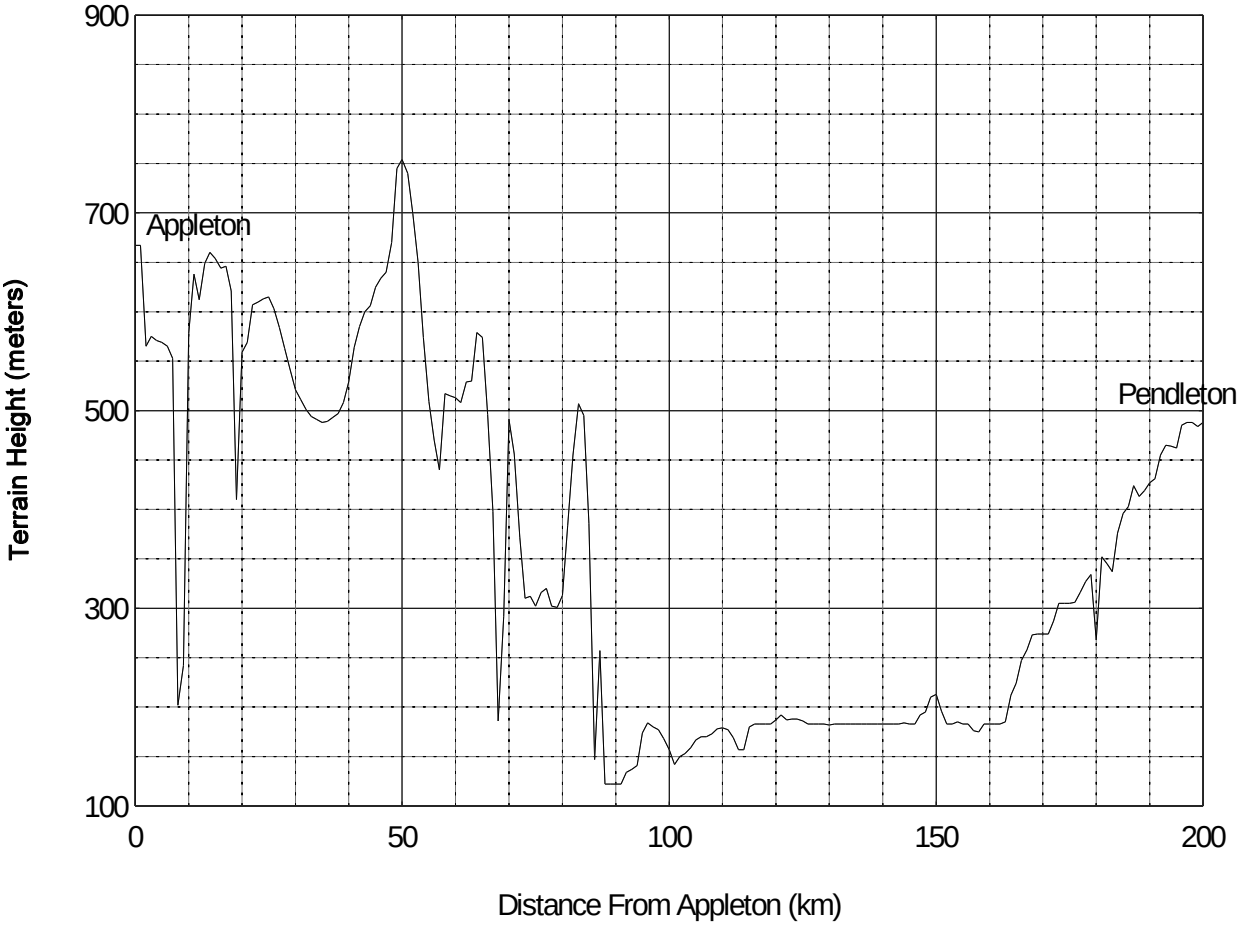



Figure 25. Terrain contour for path from Appleton to Pendleton, Washington.

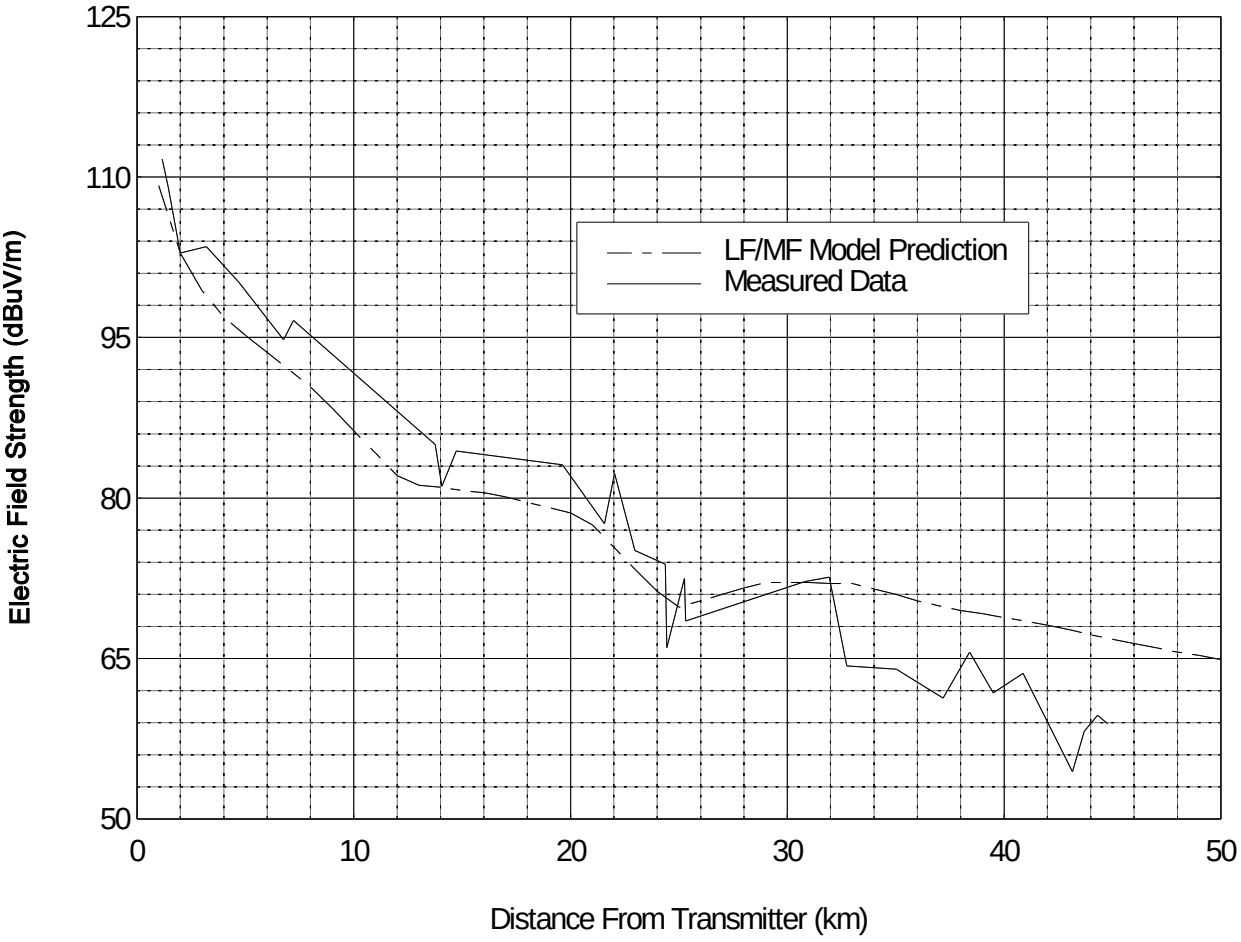



Figure 26. Comparison of measured and predicted data for Canyonlands, Utah path at 520 kHz.

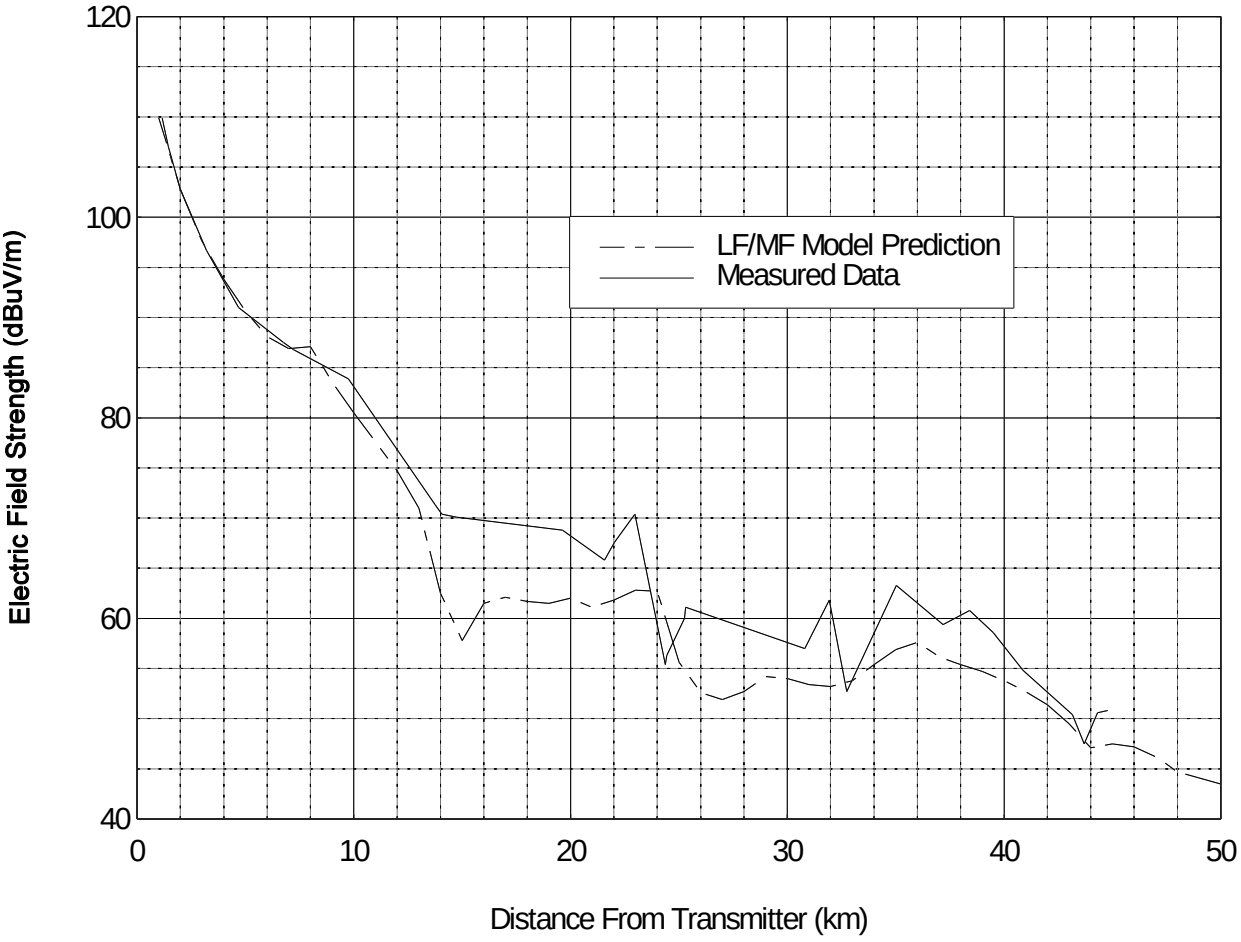



Figure 27. Comparison of measured and predicted data for Canyonlands, Utah path at 1618 kHz.

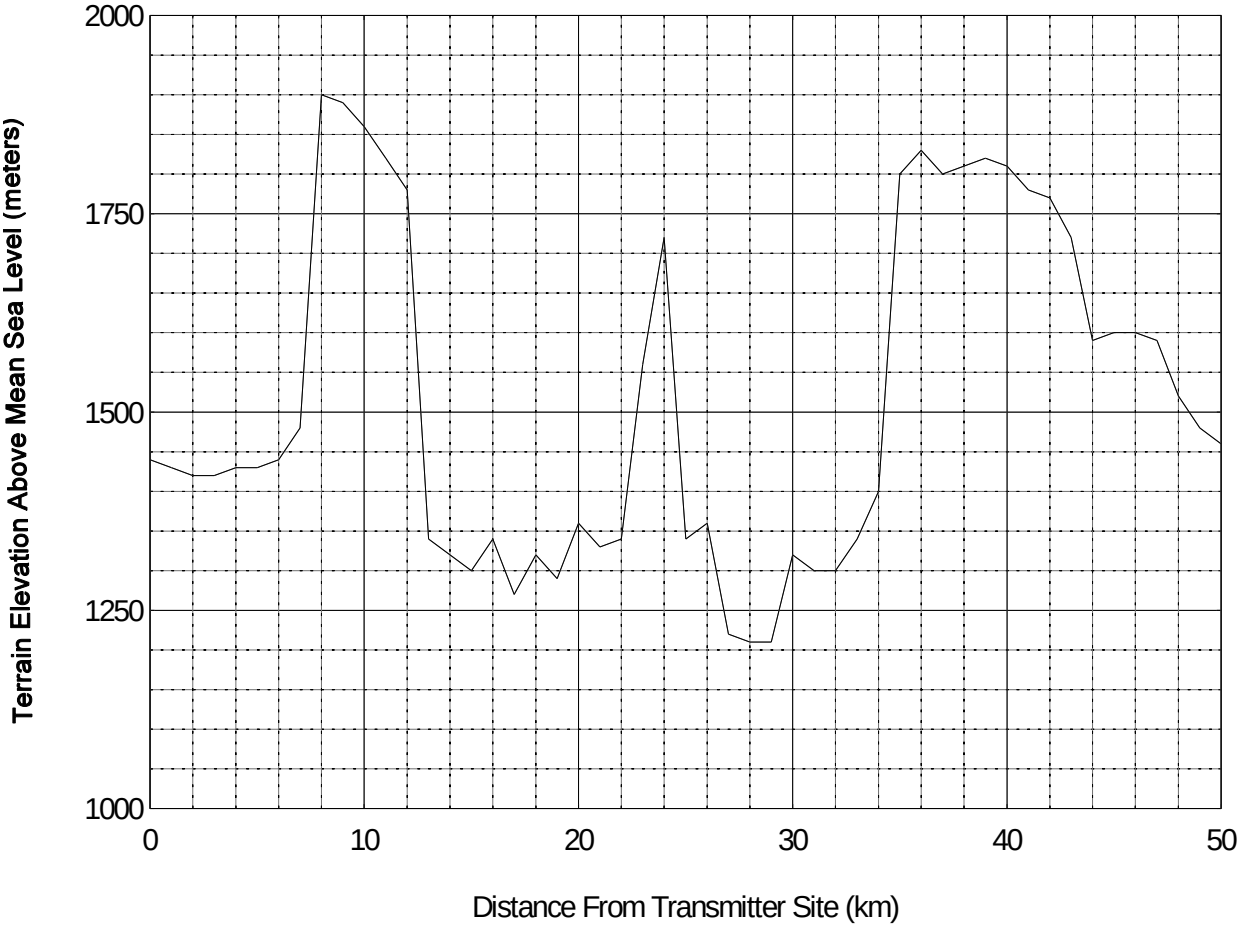



Figure 28. Terrain contour for Canyonlands, Utah measurement site.

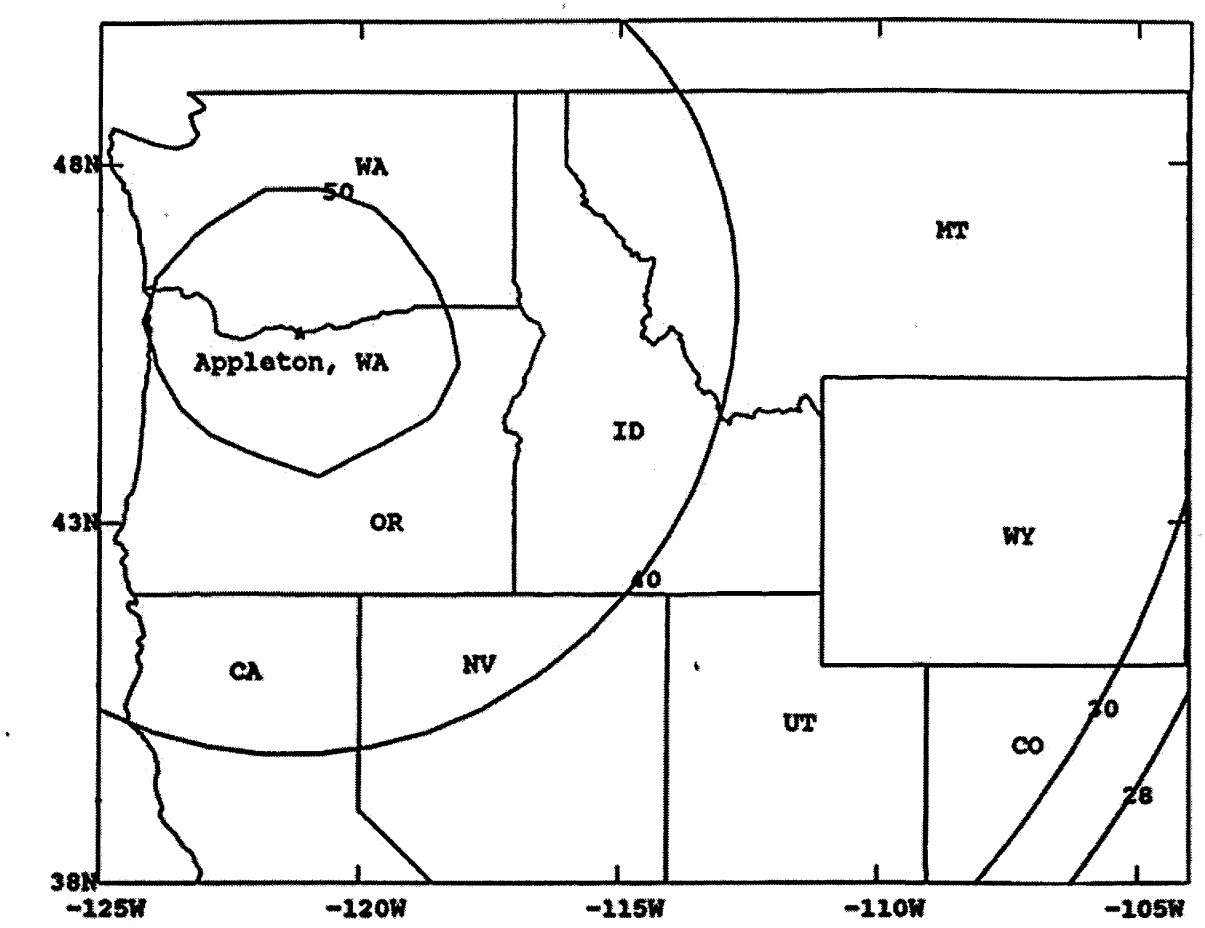



Figure 29. Contours of electric-field strength in dBuV/m from the Appleton, WA DGPS site at nighttime (f=300 kHz).

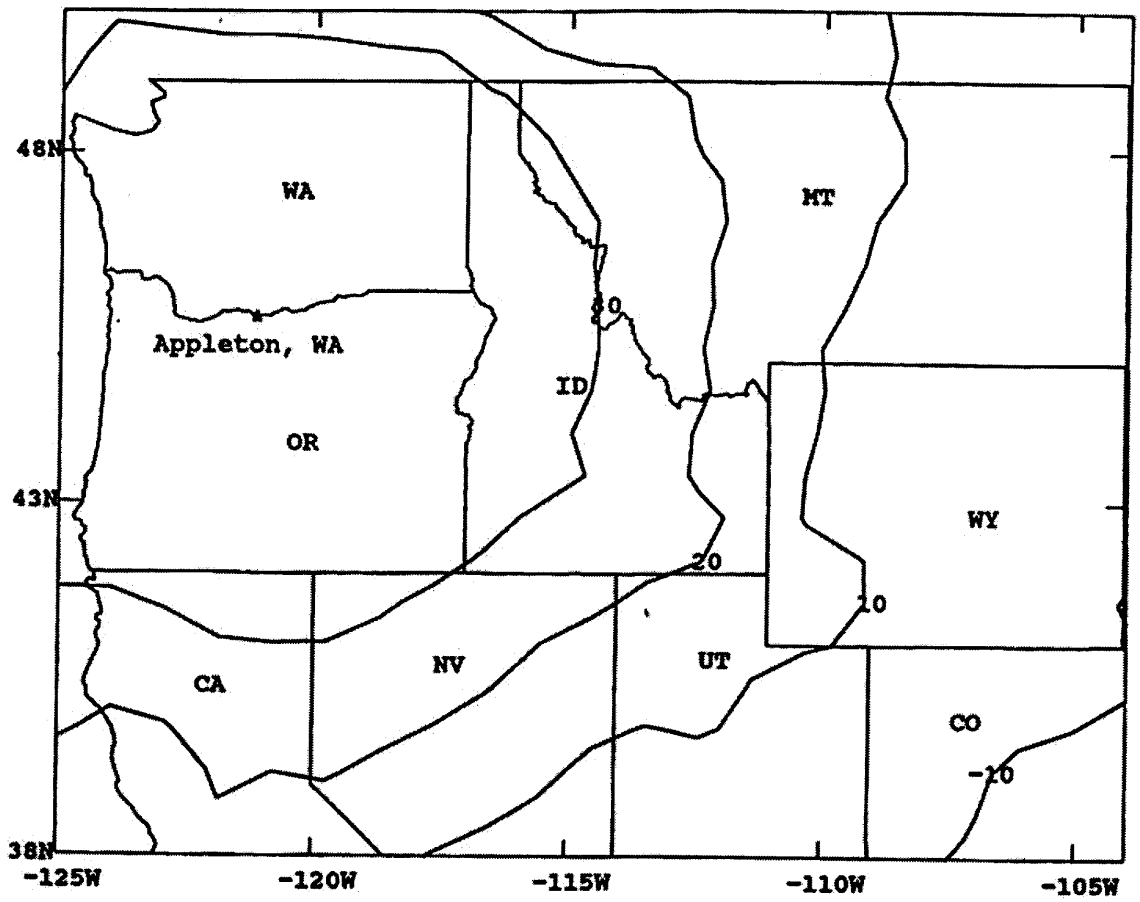



Figure 30. Contours of electric-field strength in dBuV/m from the Appleton, WA DGPS site at daytime (f=300 kHz).

## 7. CONCLUSION

This paper covered the basic aspects of radio-wave propagation and antenna modeling in the MF band. The MF band covers the frequencies of 300 to 3000 kHz. The sky wave models described in this paper are valid from 150 kHz to 1705 kHz. The ground wave models described in this paper are valid from 10 kHz to 30 MHz. In this paper the propagation models and antenna modeling techniques were shown to be quite different than those at other radio frequency bands. The propagation of radio waves in this band depends on both a ground wave and a sky wave and their interaction with the environment. The antennas are strongly influenced by the presence of ground and require numerical analysis techniques more sophisticated than free space techniques used in higher frequency bands. This paper describes radio wave propagation together with antenna

modeling in this frequency band so that a better understanding of the phenomena can be obtained for use in design and application of ITS subsystems. The models described here can be used for designing systems and making performance predictions for both of these ITS applications and any other systems that operate in this band.

The radio-wave propagation loss computed using these models is a basic transmission loss and not free-space transmission loss. Free-space is a highly idealized environment and is not the environment encountered in actual propagation situations. The ground wave includes the direct line-of-sight space wave, the ground-reflected wave, and the surface wave that diffracts around the curved Earth. Propagation of the ground wave depends on the relative geometry of the transmitter and receiver location and antenna heights in addition to the presence of a conductive Earth. The radio wave propagates as a surface wave when both the transmitter and the receiver are near the Earth in wavelengths, because the direct and ground-reflected waves in the space wave cancel each other out, and as a result the surface wave is the only wave that is left. The surface wave propagates along and is guided by the Earth's surface. As the surface wave passes over the surface of the Earth, it is attenuated as result of the energy absorbed by the Earth due to the power loss resulting from the current flowing through the Earth's resistance. Energy is taken from the surface wave to supply the losses in the ground and the attenuation of this wave is directly affected by the ground constants of the Earth along which it travels. This cancellation is a result of the fact that the elevation angle is near zero and the two ground waves (direct and reflected) are equal in amplitude and opposite in phase. This is the condition that exists for the MF band and lower frequencies. The surface wave is predominantly vertically polarized, since the ground conductivity effectively shorts out most of the horizontal electric field component. What is left of the horizontal field component is attenuated at a rate many times the vertical component of field strength. When one or both of the antennas are elevated above the ground to a significant height with respect to a wavelength, the space wave predominates.

The exact equations derived by Norton [10] can be used for analysis, or some simpler equations also by Norton [9,10] can be used to describe the flat-Earth attenuation function when the geometry is such that the flat-Earth attenuation function is appropriate. When the geometry is such that the flat-Earth attenuation function is not appropriate, then smooth-Earth, smooth-Earth mixed-path, and irregular-Earth mixed path models such as those described in this paper should be used to take into account non-zero antenna heights, mixed-path ground conditions, and terrain.

A medium frequency sky wave will be returned back to Earth by the ionosphere if the degree of ionization in the appropriate regions is sufficient to refract and reflect the incident electromagnetic wave. Ionospheric propagation models for medium frequencies can predict this degree of ionization in the different layers to determine the amount of signal that is refracted and reflected and hence the system performance. The two regions that are responsible for the refraction and reflection of medium frequencies are the D region and the E region. The first region encountered by the sky wave is the D region and the E region is located above it. The D region is a region of low electron density whose degree of ionization is determined primarily by solar photoionization. This region usually exists during the daytime and absorbs the energy in the MF radio waves that pass through it during the daytime hours. The MF sky wave is therefore highly attenuated as it passes through the D layer

during the daytime. Reflection and refraction of the sky wave by the E region does not usually occur, because of the large amount of attenuation experienced in the D region. At night the solar photoionization in the D region is reduced and hence the attenuation of the sky wave in this region is much less, so the sky wave travels on to the E region where it is refracted and reflected back to Earth. The D region of the ionosphere is characterized as having a strong dependence on frequency, but this is present only during the daytime. The E layer is the dominant contributor to LF and MF propagation at night and is only mildly dependent on frequency, so the effects of frequency on radio-wave propagation of this E layer can be neglected for most practical purposes. Three sky-wave propagation models were described in this paper and their relative merits were discussed. The ITU method is the only one that accounts for the variation of sky-wave propagation with frequency, but it has a frequency-dependent term that reduces the predicted field strength with increasing frequency. One reference, [47], notes that measurements in the United States show a frequency dependence that is exactly the opposite of what the ITU method predicts. Rather than adding the error that is incurred when using the ITU model [47], the effects of frequency for the sky wave are generally neglected. The frequency dependence over the range of 500 kHz to 1600 kHz is small, so it is often ignored and the field strength at 1000 kHz is taken as representive of the entire band [44]. The ITU method makes predictions that depend on both frequency and geomagnetic latitude. The field strength values are not symmetrical about the geomagnetic latitude equal to 0 degrees. The ITU notes that this field strength expression predicts lower field strength values as the frequency is increased in the MF band [43], but measurements performed in the United States show that the field strengths are higher at the higher frequencies in the MF band when compared to those measurements at the lower frequencies. Because of this discrepancy, the ITU method has not found wide acceptance as a worldwide prediction method. Davies [43] also refers to measurements and gives an equation that is a function of frequency. He recommends the use of predictions at 1000 kHz to represent the entire MF band. In an effort to create a valid model that would give reasonably accurate predictions in Region 2, Wang [47] developed an MF sky-wave model after examining all of the available MF methods. When compared to the ITU expression, Wang's expression is symmetrical about zero degrees latitude and is not dependent on frequency.

Accurate antenna modeling is necessary to determine the elevation and azimuth gain variability for prediction of the actual gain to be used in launching the sky wave at the appropriate take-off angles, and the ground-wave gain at the horizon angle. The performance of an antenna on or near the surface of the Earth is very dependent on the interaction with the lossy Earth. This is especially true for antennas at MF. Currently available techniques for analyzing antennas over ground with computer algorithms are time consuming and require conversion or normalization for use in system computations. This process was described in the propagation section. The gain of the antenna is a function of the antenna geometry, materials used, ground conductivity, ground dielectric constant, frequency, elevation angle, and azimuth angle. The gain required for systems performance analysis is usually calculated with respect to an isotropic radiator in free space or some other reference antenna such as a dipole. Conventional methods such as free space analysis could not be used due to the close proximity of the antennas to a lossy Earth. Antenna modeling techniques at medium frequencies must account for the actual gain that launches the ground wave. The end result for the

antenna gain described in this paper has been transformed to be referenced to an isotropic radiator in free space.

There are several methods for modeling antennas that are in close proximity to a lossy Earth. Some of these are not valid for an antenna located right on the surface and require that the antenna be 0.2 wavelengths above the surface or the algorithm used in the calculation will not be valid. These algorithms that assume free-space conditions or negligible ground effects should not be used to model antennas that are too close to the Earth, because the results are poor. The model selected for analyzing antennas makes use of extensive method-of moments calculations and is implemented in a computer program titled the Numerical Electromagnetics Code (NEC) [50]. It is an accurate method for analyzing antennas at these low and medium frequencies where the antennas are small or comparable to a wavelength in size. Numerical methods are required to solve this problem and NEC is a good algorithm to use. The NEC program operates using a computation mode that implements a Sommerfeld integral computation for the determination of electromagnetic fields for antenna structures that are buried or penetrate the ground-air interface. This computation technique includes the reflected field below the interface, the field transmitted across the interface, and the fields above the ground-air interface. The algorithms used are also valid for antennas very close to the interface. The NEC program can also model near fields of the antenna very close to the antenna structure, in addition to being able to model the far field and compute antenna gain.

A different antenna gain phenomenon occurs with antennas at medium frequencies as compared to antennas at VHF, UHF and higher frequencies. The antenna principles are the same, but the surface wave becomes more signficant at MF. This is important because it is the surface wave that accounts for practically all of the energy transmitted and received at these frequencies. The concepts of gain and efficiency for antennas close to the surface of the Earth at MF are difficult to comprehend, since a major portion of the power launched by the antenna is absorbed by the lossy Earth. A method for calculating antenna gain of MF antennas including the normalization process to interface with the propagation models has been discussed in this paper. Agreement with measurements has been shown.

The propagation and antenna models described here can be used for performance prediction of ITS applications in the roadway environment to determine design criteria and parameters for building and testing these systems. The models can also be used to resolve measurement problems. These models can also be used for performance prediction in an interference environment, and aid in the resolution of interference problems. Propagation models that are used to analyze radio communication systems require sound engineering judgement in their use for a particular analysis.

## 8. REFERENCES


[1] H.T. Friis, “A note on a simple transmission formula,” *Proc. of the IRE*, Vol. 41, May 1946, pp. 254-256.

[2] H.T. Friis, “Introduction to radio and radio antennas,” *IEEE Spectrum*, pp. 55-61, April 1971.

[3] International Telecommunications Union (ITU-R), “The concept of transmission loss,” Vol. V, ITU-R Recommendation 341-2, Dubrovnik, Yugoslavia, pp. 9-14, 1986.

[4] K.A. Norton, “Transmission loss in radio wave propagation,” *J. Res. NBS*, Vol. 63D (Radio Propagation), No. 1, pp.53-73, July/August 1953.

[5] P.L. Rice, A.G. Longley, K.A. Norton, and A.P. Barsis, “Tropospheric loss predictions for tropospheric communication circuits,” *NBS Technical Note 101*, May 1967.

[6] N. DeMinco, “Ground-wave analysis model for MF broadcast systems,” NTIA Report 86-203, Sept. 1986.

[7] E. Haakinson, S. Rothschild, and B. Bedford, “ MF broadcasting system performance model,” NTIA Report 88-237, Aug. 1988. (NTIS Order No. PB89-131411).

[8] F.E. Terman, *Electronic and Radio Engineering*, New York: McGraw-Hill Book Co., 1955, pp. 803-808.

[9] K. A. Norton, “The calculation of ground-wave field intensity over a finitely conducting spherical-Earth,” *Proceedings of the Institute of Radio Engineers*, Vol. 29, No.12, December 1941, pp. 623-639.

[10] K.A. Norton,“ The propagation of radio waves over the surface of the Earth and in the upper atmosphere,” Part I, *Proc. IRE*, Vol. 24, Oct. 1936, pp. 1367-1387; Part II, *Proc. IRE*, Vol. 25, Sept. 1937, pp 1203-1236.

[11] R. Li, “The accuracy of Norton's empirical approximations for groundwave attenuation,” *IEEE Trans. Ant. Prop.*, AP-31 , No. 4, pp 624-628, July 1983.

[12] C.A. Balanis, *Advanced Engineering Electromagnetics*, New York: John Wiley and Sons, 1989.

[13] A. Sommerfeld, “Propagation of waves in wireless telegraphy,” *Ann. D. Phys. 28*, pp. 665-736., March 1909.

[14] L.A. Berry and J.E. Herman, “A wave hop propagation program for an anisotropic ionosphere,” Office of Telecommunications Report OT/ITS RR11, 1971. (NTIS Order No. COM 75-10939/AS).

[15] L.A. Berry, "User's guide to low frequency radio coverage programs," Office of Telecommunications Technical Memorandum 78-247, January 1978.

[16] F.G. Stewart, L.A. Berry, C.M. Rush, and V. Agy, "An air-to-ground HF propagation prediction model for fast multi-circuit computation," NTIA Report 83-131, August 1983. (NTIS Order No. PB 84-145861).

[17] L.A. Berry and M.E. Chrisman, "Numerical values of the path integrals for low and very low frequencies," NBS Tech Note no. 319, 1965.

[18] L.A. Berry and M.E. Chrisman, "A Fortran program for calculation of ground-wave propagation over inhomogeneous spherical Earth for dipole antennas," NBS Report 9178, March 1966.

[19] J.R. Wait , "Electromagnetic surface waves," in *Advances in Radio Research*, J.A. Saxton (Ed.), London: Academic Press, 1964, pp. 157-217.

[20] R.J. King, "Electromagnetic wave propagation over a constant impedance plane," *Radio Science* Vol. 4, No. 3, pp.225-268, March 1967.

[21] M. Abramowitz and I.A. Stegun, *Handbook of Mathematical Functions, National Bureau of Standards AMS 55*, U.S. Government Printing Office: Washington, D.C., June 1964, pp. 297-329.

[22] V.A. Fock, *Electromagnetic Diffraction and Propagation Problems*, London: England, Pergamon Press, 1965.

[23] N. DeMinco, "Automated performance analysis model for ground-wave communication systems," NTIA Report 86-209, Dec. 1986. (NTIS Order No. PB87-164778).

[24] D.A. Hill and J.R. Wait, "Ground-wave attenuation function for a spherical Earth with arbitrary surface impedance," *Radio Science* Vol. 15, No. 3, pp. 635-643, May-June 1980.

[25] J.R. Wait, "Radiation from a vertical antenna over a curved stratified ground," *National Bureau of Standards J. Res.* Vol. 56, pp. 237-244, April 1956.

[26] J.R. Wait, "On the theory of propagation of electromagnetic waves along a curved surface," *Can. J. Phys.* Vol. 36, No. 1, pp. 9-17, June 1958.

[27] H. Bremmer, "Applications of operational calculus to ground-wave propagation, particularly for long waves," *IRE Trans. Ant. Prop*. AP-6, No. 3, pp. 267-272, 1958.

[28] H. Bremmer, *Terrestrial Radio Waves*, New York: Elsevier Publishing Company, 1949, pp. 52-85.

[29] J.R. Wait, "Radiation from a vertical antenna over a curved stratified ground,"*National Bureau of Standards, J. Res*. Vol. 56, pp237-244, 1956.

[30] J.R. Wait, "On the theory of propagation of electromagnetic waves along a curved surface," *Can. J. of Phys.* 36, Vol. 1, pp9-17, 1958.

[31] G. Millington, "Ground wave propagation over an inhomogeneous smooth Earth," *J. IEE* (London), Part IV, 96, pp. 225-268, March 1949.

[32] J.R. Wait and D.A. Hill, "Excitation of the HF surface wave by vertical and horizontal antennas," *Radio Sci.* Vol. 14, No. 5, pp 767-780, Sept-Oct 1979.

[33] D.A. Hill, "HF ground wave propagation over forested and built-up terrain," NTIA Report 82-114, Dec. 1982, (NTIS order No. PB 83-194175).

[34] R.H. Ott, "A new method for predicting HF ground-wave attenuation over inhomogeneous irregular terrain," Office of Telecommunications Research Report 7, 1971 (NTIS Order No. AD721179).

[35] C. Wagner, "On the numerical solution of Volterra integral equations," *J. Math. Phys*., Vol. 32, pp. 289-401, 1953.

[36] R.H. Ott, "An alternative integral equation for propagation over irregular terrain," Part 2, *Radio Sci.* Vol. 6, Number 4, pp 429-435, April 1971.

[37] R.H. Ott and L.A. Berry, "An alternative integral equation for propagation over irregular terrain," Part 1, *Radio Sci*., Vol. 5, No. 5, pp 767-771, May 1970.

[38] S. Rotheram, J.D. Milsom, R.N. Herring, J.M. Pielou, and K.S. Gill, "Ground-wave propagation over irregular surfaces," *Proceedings of the Fourth International Conference on Antennas and Propagation (ICAP 85) (Proceedings No. 248)*, 1985, Coventry, England, (Published by the IEE), April 16-19, 1985.

[39] J.E. Adams, J.C. Carroll, E.A. Costa, D.R. Ebaugh Jr., J.R. Godwin, E.J. Haakinson, D.H. Layton, and D. Smith, "Measurements and prediction of HF ground-wave propagation over irregular, inhomogeneous terrain," NTIA Report 84-151, July 1984. (NTIS Order No. PB 85-119666).

[40] R.H. Ott, L.E. Vogler, and G.A. Hufford, "Ground-wave propagation over irregular, inhomogeneous terrain: Comparison of calculations and measurements," NTIA Report 79-20, May 1979. (NTIS Accession No. PB 298668/AS).

[41] D.G. Fink and D. Christiansen (editors), *Electronic Engineers Handbook*, Chapter 18 "Radio-Wave Propagation" by R.C. Kirby, New York: McGraw-Hill Book Co., pp. 18-96 to 18-103, 1989.

[42] K. Davies, *Ionospheric Radio Propagation*, *NBS Monograph 80* (U.S. Government Printing Office), Washington, DC, pp. 2-7, 1965.

[43] ITU-R (International Telecommunications Union), (CCIR-International Radio Consultative Committee), "Sky-wave field strength prediction method for the broadcasting service in the frequency range 150 to 1600 kHz," Recommendation 435-7, International Telecommunications Union, Geneva, Switzerland, 1992.

[44] K. Davies, *Ionospheric Radio*, Chapter 11, London: Peter Peregrinus Ltd, 1990, pp.408-440.

[45] ITU (International Telecommunications Union), Final Acts of the Regional Administrative MF Broadcasting Conference (Region 2), Rio de Janeiro, 1981 (International Telecommunication Union, Geneva, Switzerland).

[46] CCIR (International Radio Consultative Committee), "Prediction of sky-wave field strength between 150 and 1600 kHz," CCIR Recommendation 435-5, Vol. VI, International Telecommunication Union, Geneva, Switzerland (NTIS Order No. PB-87-14117-2), 1986.

[47] J.A. Wang, "A skywave propagation study in preparation for the 1605-1705 kHz broadcasting conference," *IEEE Trans. Broadcasting*, BC-31, No. 1, pp. 10-19, March 1985.

[48] M. Pokempner, "Comparison of available methods for predicting medium frequency sky-wave field strengths," NTIA Report 80-42, 1980. (NTIS Order No. PB 80-211444)

[49] J.A. Wang, "Diurnal variation in skywave propagation," Technical Memorandum FCC/OST TM 83-4, June 1983.

[50] G.J. Burke, "Numerical Electromagnetic Code- NEC-4, method of moments Parts I and II," University of California Lawrence Livermore National Laboratory Report UCRL-MA-109338, Livermore, CA January 1992.

[51] G.J. Burke and E.I. Miller, "Modeling antennas near to and penetrating a lossy interface," Lawrence Livermore National Laboratory, UCRL-89838, Livermore, California, 1983.

[52] K.A. Norton, "Transmission loss in radio propagation-II," *NBSA Tech. Note No. 12*, 1959.

[53] R.C. Fenwick and W.L.Weeks, "Submerged antenna characteristics," *IEEE Trans. Ant. Prop.*, AP-11, pp. 296-305, May 1963.

[54] E.C. Jordan, "*Electromagnetic Waves and Radiating Systems*," New Jersey: Prentice Hall, pp.608-655, 1950.

[55] J.R. Hoffman, J.J. Lemmon, R.L. Ketchum,“DGPS field strength measurements at a GWEN site,” NTIA Report 98-346, April 1998. (NTIS Order No. PB 98-138928).

[56] J.R. Hoffman, J.J. Lemmon, R.L. Ketchum,“ Field strength measurements of DGPS and FAA beacons in the 285- to 325-kHz band,” NTIA Report 97-337, June 1997. (NTIS Order No. PB 97-176408).